

The link between the masses and central stellar populations of S0 galaxies

A.G. Bedregal^{1*}, A. Aragón-Salamanca¹, M.R. Merrifield¹ and N. Cardiel²

¹*School of Physics and Astronomy, University of Nottingham, University Park, Nottingham, NG7 2RD, UK*

²*Departamento de Astrofísica, Facultad de Físicas, Universidad Complutense de Madrid, 28040 Madrid, Spain*

Accepted ***. Received ***; in original form ***

ABSTRACT

Using high signal-to-noise ratio VLT/FORS2 long-slit spectroscopy, we have studied the properties of the central stellar populations and dynamics of a sample of S0 galaxies in the Fornax Cluster. The central absorption-line indices in these galaxies correlate well with the central velocity dispersions (σ_0) in accordance with what previous studies found for elliptical galaxies. However, contrary to what it is usually assumed for cluster ellipticals, the observed correlations seem to be driven by systematic age and α -element abundance variations, and not changes in overall metallicity. We also found that the observed scatter in the index– σ_0 relations can be partially explained by the rotationally-supported nature of these systems. Indeed, even tighter correlations exist between the line indices and the maximum circular velocity of the galaxies. This study suggests that the dynamical mass is the physical property driving these correlations, and for S0 galaxies such masses have to be estimated assuming a large degree of rotational support. The observed trends imply that the most massive S0s have the shortest star-formation timescales and the oldest stellar populations.

Key words: galaxies: elliptical and lenticular – galaxies: stellar populations

1 INTRODUCTION

This is the third paper of a series designed to study S0 galaxies in the Fornax Cluster by using optical, long-slit spectroscopy (VLT/FORS2) and archive optical and near-infrared imaging. In Bedregal et al. (2006a, hereafter Paper I) we described the sample and studied the stellar kinematics along the apparent semimajor axes of these objects. In Bedregal et al. (2006b, hereafter Paper II) we use the circular rotational velocities obtained in Paper I to study the Tully-Fisher relation (Tully & Fisher 1977) of these galaxies as part of a larger compiled sample of ~ 60 local S0s. In this paper we study the sample of Fornax S0s and try to establish links between the properties of their central stellar populations (ages, chemical abundances) and their global properties such as mass and dynamics. The ultimate goal is to find the main physical drivers governing the formation and evolution of S0s.

Many previous works on stellar populations of early-type galaxies have concentrated on the relations between velocity dispersion and Mg indices (e.g. Terlevich et al. 1981; Gorgas et al. 1990; Guzmán et al. 1992; Bender et al. 1993; Jorgensen et al. 1996; Bender et al. 1998; Bernardi

et al. 1998; Colless et al. 1999; Jorgensen 1999; Kuntschner 2000; Poggianti et al. 2001; Mehlert et al. 2003; Thomas et al. 2004), which are usually interpreted as correlations between mass and metallicity. However, there is still controversy about the role of relative ages and abundances of different elements in the observed trends (Jorgensen 1999; Trager et al. 1998, 2000; Kuntschner et al. 2001; Poggianti et al. 2001; Mehlert et al. 2003; Thomas et al. 2005) with some recent results pointing to an important dependence of these relations on both age and α -element abundances (Gallazzi et al. 2006; Sánchez-Blázquez et al. 2006).

The vast majority of these studies bundle together ellipticals and S0s treating them as a single population of ‘early-type’ galaxies. Here we concentrate on S0s as a distinct class. Their formation history could be very different from that of ellipticals even though some of their properties may appear similar (see, e.g., Aragón-Salamanca, Bedregal and Merrifield 2006). By using a full set of 10 absorption line indices and careful comparison with the results from stellar population synthesis models we will try to break the degeneracies between age, overall metallicity and α -element abundances.

The remainder of the paper is laid out as follows. In Section 2, we describe the different steps followed to obtain accurate Lick absorption line indices. In Section 3 we make

* E-mail: bedregal@damir.iem.csic.es

some tests in order to compare Lick index measurements at different spectral resolutions. In Section 4 we make consistency checks between the data and the Bruzual & Charlot (2003) models. Section 5 presents the main results and then discusses their implications. Finally in Section 6 our conclusions are summarised.

2 THE DATA: LINE INDEX MEASUREMENT

In this section, the main steps followed to calculate Lick/IDS line-strength indices (Burstein et al. 1984, 1986; Worthey et al. 1994; Worthey & Ottaviani 1997) using long-slit spectra are described. This will allow us to study scaling relations such as the one between Mg_2 and central velocity dispersion (e.g. Burstein et al. 1988; Guzmán et al. 1992; Bender, Burstein & Faber 1993) and to compare the results to predictions from simple stellar population models of Bruzual & Charlot (2003, hereafter BC03).

The basic data reduction and extraction of the kinematics are described in Paper I. The only change introduced at this level is a new criterion for the binning process, following the precepts of Cardiel et al. (1998). The aim of this procedure is to estimate the minimum signal-to-noise ratio (S/N) required for the new bins in order to obtain reasonably small uncertainties in $H\beta$ line strength measurements ($\delta(H\beta)$ between 0.04 and 0.3) and so, in the relative ages. An estimate of the minimum $\delta(H\beta)$ was made for each galaxy by using different $H\beta$ -versus-metallic-index diagrams and BC03 model grids; depending on the position of the galaxies' data points on the grids, a given uncertainty in the indices will translate into a corresponding error in age. In the majority of cases, an uncertainty no larger than 4 Gyr was allowed for the outermost bins. Then, the following expression of Cardiel et al. was used to obtain the S/N required for a given uncertainty $\delta(H\beta)$:

$$S/N[\text{\AA}] = \frac{7.301 - 0.2539 \cdot H\beta}{\delta(H\beta)} \quad (1)$$

The S/N per \AA of the new bins are 100, 50 and a minimum of ~ 30 (this last value varying somewhat from galaxy to galaxy), decreasing as the radius increases. As a result of the new binning, the data cover median radii ~ 2 bulge effective radius (R_e) for this sample of S0s.

2.1 Transformation to the Stellar Library Resolution

The Lick/IDS indices studied are listed in Table 1. To be able to compare the results to simple stellar population models, the indices must be measured at the same spectral resolution as the model's stellar libraries. The width of the observed spectral lines are a convolution between the instrumental width and the velocity dispersion of the stars projected along the line-of-sight. Therefore, to transform the galaxies' spectra to the required resolution, they were convolved with a Gaussian of dispersion, σ , equal to

$$\sigma = \sqrt{\sigma_{\text{lib}}^2 - \sigma_{\text{inst}}^2 - \sigma_{\text{gal}}^2}, \quad (2)$$

where σ_{lib} is the resolution from the stellar library, σ_{inst} is the instrumental widening ($\sim 30 \text{ km s}^{-1}$, see Paper I) and

Table 1. Lick indices used in this study (Worthey et al. 1994; Worthey & Ottaviani 1997) and resolution at which each index was measured when Lick resolution was adopted (Sánchez-Blázquez 2004).

Index	Lick Resol. [km s^{-1}]
$H\beta$	225
Fe5015	200
Mg_1	200
Mg_2	200
Mgb	200
Fe5270	200
Fe5335	200
Fe5406	200
Fe5709	200
Fe5782	200

σ_{gal} is the velocity dispersion of the galaxy at the corresponding radius, already calculated during the extraction of the kinematics.

Once the spectra were broadened, line-strength indices were measured in the central regions of the galaxies (within $R_e/8$ of the bulge) using the software **INDEXF**, developed by one of us (NC¹). Following the Lick/IDS index definition, the program calculates a *pseudocontinuum* (a local continuum level) for each spectral feature defined by the means within two pseudocontinuum bands located one at each side of the spectral feature (see Worthey et al. 1994 and Worthey & Ottaviani 1997). Then, the line index is measured with respect of the pseudocontinuum by integrating within the feature central band

$$\text{Index} = \int_{\lambda_{c1}}^{\lambda_{c2}} \left(1 - \frac{S_\lambda}{C_\lambda}\right) d\lambda, \quad (3)$$

where λ_{c1} and λ_{c2} are the initial and final wavelengths of the central band, S_λ is the flux of the spectrum at a certain λ and C_λ is the corresponding pseudocontinuum flux. This program also estimates the uncertainties resulting from the propagation of random errors and from the effect of uncertainties on radial velocity by performing Monte-Carlo simulations.

The choice of BC03 models instead of other alternatives, like the models of Thomas, Maraston & Bender (2003, hereafter TMB03), was made based on the higher resolution of the stellar libraries of the former (3 \AA , Le Borgne et al. 2003), which permitted the study of the spectral features of these galaxies in greater detail. For the study of the main stellar population properties, however, a BC03 model with Lick resolution had to be used (resolution from FWHM $\sim 11 \text{\AA}$ around 4000 \AA to $\sim 8.5 \text{\AA}$ around 5000 \AA) given the higher reliability of these models when individual ages and metallicities are estimated². We emphasise that at both, Lick and

¹ <http://www.ucm.es/info/Astrof/software/indexf/indexf.html>

² The Lick resolution models make use of the so-called *fitting functions* (Worthey et al. 1994; Worthey & Ottaviani 1997) while the 3 \AA models don't. As a result, the model grids of the later sometimes show irregular (unphysical) patterns which translate in very uncertain individual ages and [Fe/H].

3 Å resolutions, we are using directly the predictions provided from BC03. The normal distribution of BC03 models includes predictions for both spectral resolutions, so we refer the reader to BC03 paper for further details concerning these models. In synthesis, all indices were measured at both resolutions by applying the previously described procedures. Further comparisons between the two index sets are presented in the following sections.

For NGC 1316, NGC 1380 and NGC 1381, the velocity dispersions within their central regions are higher than the 3 Å stellar library's resolution. Therefore, the procedure described above cannot be applied and the indices must be corrected after they have been measured. In these cases, we proceed as follows: for each galaxy, the best stellar-template combination for the affected bins were used as a model of the non-convolved galaxy spectra. Using equation 2, these spectra were widened to the stellar library resolution and then, in steps of 20 km s^{-1} , convolved with Gaussians of dispersions σ_{gal} between 0 and 400 km s^{-1} . The next step consisted of measuring all line indices in each spectrum and calculate a correction factor for each index, $C(\sigma)_{\text{Index}}$, of the form

$$C(\sigma)_{\text{Index}} = \text{Index}(0)/\text{Index}(\sigma). \quad (4)$$

$\text{Index}(0)$ is the index measured from the best stellar-template combination degraded at the stellar library resolution, and $\text{Index}(\sigma)$ is the index measured from the same spectrum but widened by $\sigma \text{ km s}^{-1}$. Therefore, the corrected index is given by

$$\text{Index}(0) = C(\sigma)_{\text{Index}} \cdot \text{Index}(\sigma). \quad (5)$$

Notice, however, that for the molecular indices Mg_1 and Mg_2 , measured in magnitudes, the correction applied was of the form

$$C(\sigma) = \text{Index}(0) - \text{Index}(\sigma). \quad (6)$$

The correction factors for the individual bins turned out to be similar within each galaxy. Therefore, it was decided to apply a single set of correction factors for each S0 by taking the average of the individual bins' corrections and fitting the results with polynomials of order 3. For NGC 1316 and 1380, analogous corrections were applied when Lick resolution was used.

The corrections were applied along the radius, R , to all spectral bins for which the velocity dispersion was higher than the stellar library's resolution ($\sigma_{\text{gal}}^2(R) + \sigma_{\text{inst}}^2 \geq \sigma_{\text{lib}}^2$). For NGC 1380 and NGC 1381 the different corrections ranged between 2–10% of the value of the measured indices, while for NGC 1316 they were slightly larger, typically between 10–20% of the original measurements. For each galaxy, an estimate of the uncertainty in these corrections was attempted by measuring the deviations of all the coefficients $C(\sigma)_{\text{Index}}$ from each bin at a velocity dispersion of 400 km s^{-1} . The resulting errors translate into uncertainties of the order of 0.001 Å for the different indices. Such errors are negligible compared to other sources of error from the data reduction/kinematics extraction processes, and so were neglected in subsequent analysis.

2.2 Emission and Lick Spectrophotometric Corrections

For a long time early-type galaxies were considered as gas/dust free objects. However, subsequent work on large samples of ellipticals has revealed that about 50% of these objects show weak nebular emission lines in their optical spectra (Caldwell et al. 1984; Phillips et al. 1986; Goud-frooij et al. 1994). Measurements of different nebular lines indicates the presence of 10^3 – 10^5 M_{\odot} of ionised gas in the central regions of these galaxies. Despite the small amount of gas, some absorption line features can be affected by these emissions.

Weak traces of nebular emission ($[\text{OIII}]_{\lambda 5007}$ rest frame) were found in the spectra, which affects the measurement of the indices Fe5015 (within its central band) and Mgb (within one of the pseudocontinuum bands). To correct these indices of emission, the best stellar-template combination was compared to the galaxy spectrum and the spectral feature of $[\text{OIII}]_{\lambda 5007}$ was replaced by the corresponding section of the best stellar-template combination before the indices were calculated. No other signatures of emission, such as $[\text{OIII}]_{\lambda 4959}$ or $[\text{NI}]_{\lambda 5200}$, were found which could affect the measurements of other metallic indices.

It was also found that the index $\text{H}\beta$ has traces of contamination from emission. The correction of this index is of particular importance in this study given that it is the main age indicator. The presence of emission in $\text{H}\beta$ decreases the magnitude of the measured index and the inferred age becomes older ($\text{H}\beta$ decreases with the age of the stellar population). González (1993), studying a sample of bright elliptical galaxies, found an empirical correlation between the $\text{EW}[\text{OIII}]_{\lambda 5007}$ and the EW of $\text{H}\beta$ in emission. For his brightest galaxies he found that $\frac{\text{H}\beta_{\text{emission}}}{\text{EW}[\text{OIII}]_{\lambda 5007}} \sim 0.7$. However, Trager et al. (2000) found in a sample of 27 elliptical galaxies that this relation has variations between 0.33 and 1.25, and that the mean value is 0.6 instead of 0.7. Accordingly, it was decided to apply the following (additive) emission correction for the index $\text{H}\beta$:

$$\Delta(\text{H}\beta) = 0.6 \cdot \text{EW}[\text{OIII}]_{\lambda 5007}, \quad (7)$$

where $\text{EW}[\text{OIII}]_{\lambda 5007}$ was measured from the residual spectra obtained by subtracting the best combinations of stellar templates from the galaxy spectra. The variations found by Trager et al. (2000) in the ratio $\text{H}\beta/[\text{OIII}]_{\lambda 5007}$ are translated into uncertainties in the determination of the age of the order of 3%, negligible compared to other sources of error for this index. For the S0 galaxies analyzed here, the corrections applied to $\text{H}\beta$ were not usually larger than 10% of the original measurements.

When models based on Lick/IDS libraries (e.g. some of the models published by BC03, TMB03) are used, a spectrophotometric correction is usually applied to the measured indices. This is because the Lick libraries are not calibrated in flux, but flux-normalised by using a tungsten lamp. The indices are usually corrected by additive factors calculated from observations of stars from the Lick library with the same instrumental configuration and photometric conditions as the data. We lack such data in the current study; however, there are other ways around this issue. We attempt to calibrate our Lick resolution indices by using data from the literature. In his sample of early-type galaxies, Kuntschner

(2000) presents lower resolution, fully calibrated central line indices for our entire sample of S0s, being an ideal dataset for our purpose. All our indices but Fe5782 were also measured in his work. We rebinned our data by using a central aperture of 3.85" as in Kuntschner (2000) in order to perform the comparison. By using the individual measurements for each galaxy, mean corrections (offsets) were estimated for each index. The uncertainties of these corrections, however, were quite large. After studying the significance of the offsets by using a Student-t correlation test, we conclude that for all the indices but Mg₁ and Mg₂ the offsets were not significant at 95% confidence level. These two molecular indices are the most likely to be affected by spectrophotometric calibration problems given their highly separated pseudocontinuum bands. In any case, the corrections estimated for the remaining indices were usually far below 10% the value of the original measurements. Therefore, we only applied the corrections to the Mg₁ and Mg₂ indices measured at Lick resolution:

$$\delta(\text{Mg}_1)_{\text{Lick}} = +0.0166 \pm 0.0056 \text{ mag} \quad (8)$$

$$\delta(\text{Mg}_2)_{\text{Lick}} = +0.0216 \pm 0.0072 \text{ mag}. \quad (9)$$

We stress that these corrections were applied only to Lick resolution measurements. The stellar libraries on which 3 Å resolution models are based have been properly calibrated, so no corrections are required for 3 Å resolution data.

In this work, two combined indices were also used, $\langle \text{Fe} \rangle$ (Gorgas, Efsthathiou & Aragón-Salamanca 1990) defined as

$$\langle \text{Fe} \rangle = \frac{\text{Fe}5270 + \text{Fe}5335}{2}, \quad (10)$$

and $[\text{MgFe}]'$ (González 1993; Thomas, Maraston & Bender 2003) defined as

$$[\text{MgFe}]' = \sqrt{\text{Mgb} \cdot (0.72 \times \text{Fe}5270 + 0.28 \times \text{Fe}5335)}. \quad (11)$$

$[\text{MgFe}]'$ will be particularly important for the analysis of stellar population parameters, like age and metallicity, given its almost null dependency on α -element abundance (TMB03). All measured and corrected central indices for the Fornax sample are presented in Tables A1 (at 3 Å resolution) and A2 (at Lick resolution) in the Appendix.

Finally, note that in different parts of this work the atomic indices are sometimes expressed in magnitudes (following Colless et al. 1999) according to the expression

$$\text{Index}^* = -2.5 \cdot \log \left(1 - \frac{\text{Index}}{\Delta\lambda} \right), \quad (12)$$

where Index^* represents the index in magnitudes, Index is the index expressed in Å, and $\Delta\lambda$ is the central bandwidth in Å, listed in Table 1 of Worthey et al. (1994). In the particular case of $\langle \text{Fe} \rangle$, the index in magnitudes was calculated using

$$\langle \text{Fe} \rangle^* = -2.5 \cdot \log \frac{1}{2} \left(1 - \frac{\text{Fe}5270}{\Delta\lambda_{\text{Fe}5270}} - \frac{\text{Fe}5335}{\Delta\lambda_{\text{Fe}5335}} \right), \quad (13)$$

while $[\text{MgFe}]'$ was always expressed in Å.

3 COMPARISON BETWEEN INDICES AT DIFFERENT RESOLUTIONS

In this section, comparisons between line indices measured at different resolutions are made in order to understand in

a qualitative way the possible effects on the ages and metallicities when inferred from degraded spectra. In Figure 1, measurements of all central indices at 3 Å and Lick resolution are compared for the whole galaxy sample.

All forthcoming comparisons are made in relation to the 3 Å indices. The $\text{H}\beta$ index suffers little degradation, where only the galaxy NGC 1375, with the strongest $\text{H}\beta$ -absorption, may suffer from a small relative decrement of its luminosity-weighted age estimate. The Mg indices suffer a dissimilar behaviour. While Mgb presents a very little variation between the two resolutions, the molecular indices Mg₁ and Mg₂ show a systematic offset with respect to the 1:1 lines. Their larger values at Lick resolution are just a consequence of applying the spectrophotometric correction in Section 2.2. In general, Fe indices present systematic shifts with respect to the 1:1 lines with slightly larger differences for galaxies with strong spectral features. The dependence on index intensity may introduce some differences in the relative metallicities derived using Fe features by diminishing this parameter in galaxies with strong Fe lines. However, the relative differences in shifts among the galaxies are not strong enough to make this an important effect. The relative index variations between galaxies can be more easily appreciated in Figure 2, where the indices at 3 Å resolution are plotted versus the fractional change when they are measured at Lick resolution.

The Fe features vary, on average, by -15% , while the $\text{H}\beta$ and the Mgb index variations are usually less than -10% . The corresponding panels for Mg₁ and Mg₂ illustrate not only the systematic offsets of Figure 1 but the magnitude of the spectrophotometric corrections applied to these two indices. The variations are particularly important for Mg₁, where a median percentual change of $+20\%$ is found. This is the main reason why we are going to restrict the use of Mg₁ and Mg₂ to the *qualitative* tests presented in the following sections, without attempting to estimated individual ages and $[\text{Fe}/\text{H}]$ with them. In this way, Mgb becomes our more reliable magnesium tracer. Concerning the estimate of the $[\text{Mg}/\text{Fe}]$ (or $[\alpha/\text{Fe}]$) relative abundance tracers, the fact that the Mgb index presents little variation in comparison to the Fe indices will certainly introduce changes for each individual galaxy if the abundance tracers are measured as the differences between metallicities (e.g. $[\text{Fe}/\text{H}]_{\text{Mgb}} - [\text{Fe}/\text{H}]_{\langle \text{Fe} \rangle}$). However, the similar variations in the Fe indices experienced by all the galaxies will result in the *relative* $[\text{Mg}/\text{Fe}]$ abundances between them being mostly unaffected. In any case, the index ratio $\text{Mgb}/\langle \text{Fe} \rangle$ provides an alternative model-independent tracer of the α -element abundances previously applied by other authors (see TMB03).

In summary, in this section comparisons between line indices measured at 3 Å and Lick resolution have been made in order to find possible systematic differences which could affect our conclusions when one set or the other is used. Negligible variations are found in the $\text{H}\beta$ and Mgb indices. A somewhat larger change is detected in the Fe features, but we conclude that such effects will not introduce important *relative* changes in the ages, metallicities and abundance tracers between the galaxies.

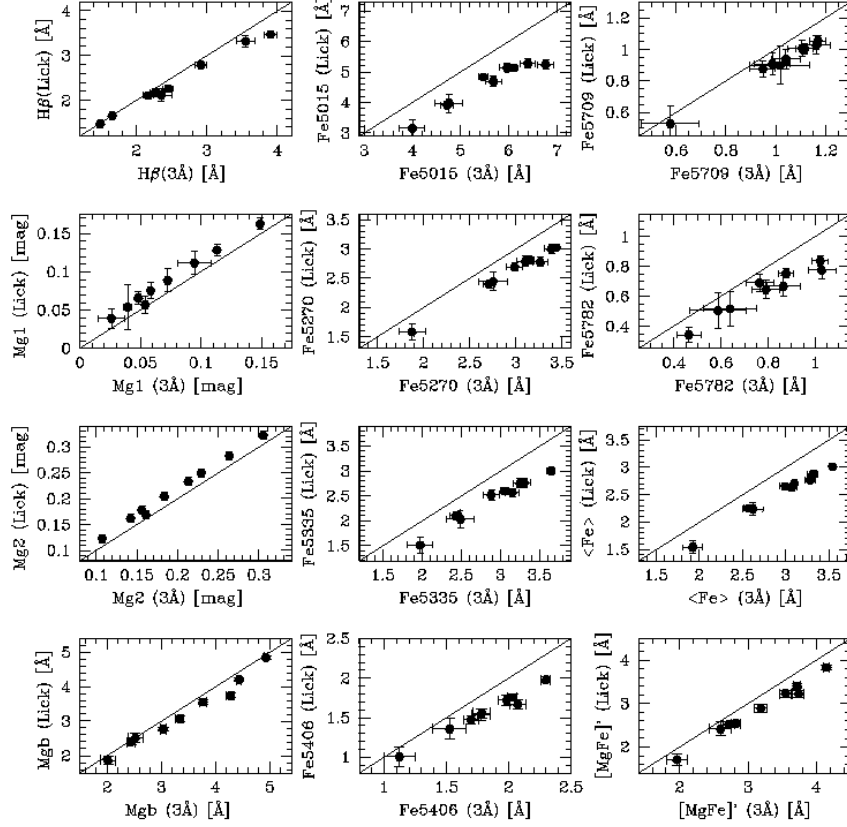


Figure 1. Comparison of the central line indices measured at 3 Å and Lick resolutions.

4 THE MODELS: CONSISTENCY WITH THE DATA

Before showing the main results, in this section some consistency checks between the BC03 models and the data are presented. These tests give an idea of how well the models describe the data and, in consequence, how the model results should be interpreted. For a stellar population study, it is important to check if there are significant differences in the relative spectrophotometric calibrations of the data and the stellar libraries used by the models. If differences are found, the results must be interpreted accordingly. Although ages and metallicities were estimated using Lick resolution data and models, some qualitative comparisons were also made with the higher resolution data. Therefore, the consistency tests were performed for both the 3 Å and Lick resolution BC03 models and data sets.

4.1 3 Å resolution models and data

When using the 3 Å resolution STELIB library, it is expected that little difference from the data will be found because both sets of spectra were flux calibrated using spectrophotometric standard stars.

This assumption was tested by creating index–index plots which are almost degenerate in age and metallicity. In this way, the model grids describe narrow bands in the

index–index space, regions which should trace the galaxies’ data if the models describe accurately the properties of these objects and if there are no problems with the relative flux calibrations.

In Figure 3, different Mg indices are plotted against each other. The folded grids represent BC03 3 Å resolution models, and the line indices measured within $R_e/8$ are plotted for the complete S0 sample. The match between data and models is very good, with a hint of a small systematic deviation for galaxies with intense Mg indices (NGC 1316, 1380 and 1381). Even less pronounced, a small offset towards lower Mg_1 values is apparent from the Mg_1 versus Mgb panel. A similar plot is presented in Figure 4 for six Fe indices. In these cases, the scatter from the models is larger than for the Mg indices, but the models seem to trace the mean trends in the data. For the three plots with Fe5015, however, there seems to be some systematic deviation between the data and model grids. Because the central band-pass of Fe5015 was corrected from $[OIII]_{\lambda 5007}$ emission, this particular index must be used with caution.

Thus, as predicted, no important mismatches were found between indices and model predictions at 3 Å resolution, suggesting that the relative flux calibrations are consistent with each other. By assuming solar abundances, BC03 models are able to consistently reproduce the observations for the majority of these S0 galaxies. Therefore, in the fol-

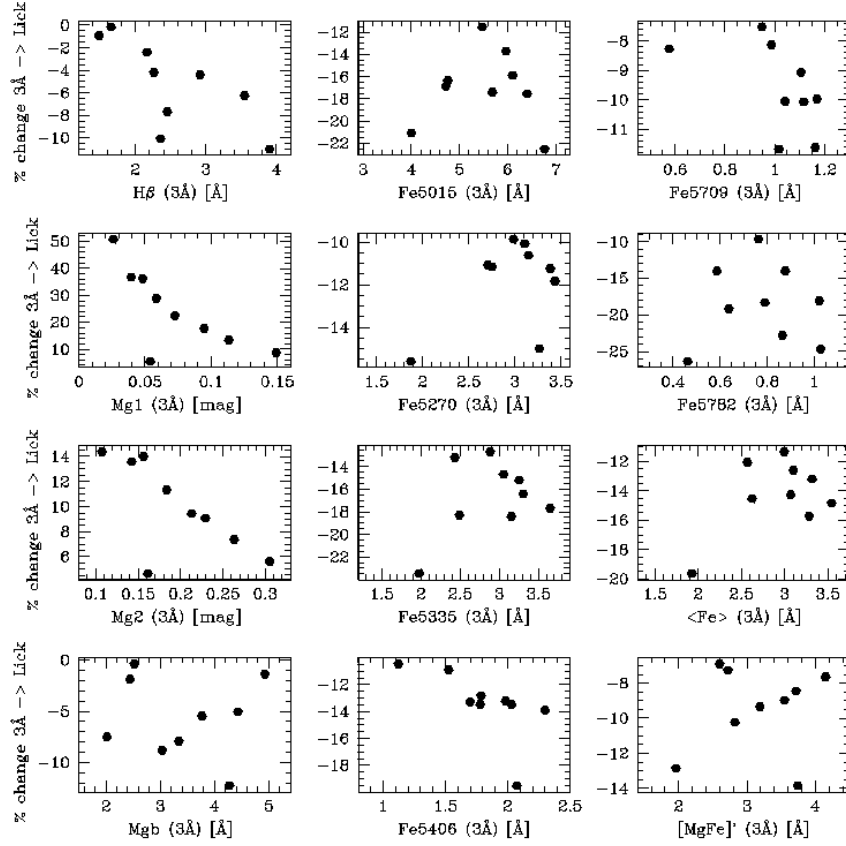


Figure 2. Central line indices at 3 Å resolution versus fractional change (%) when measured at the Lick resolution.

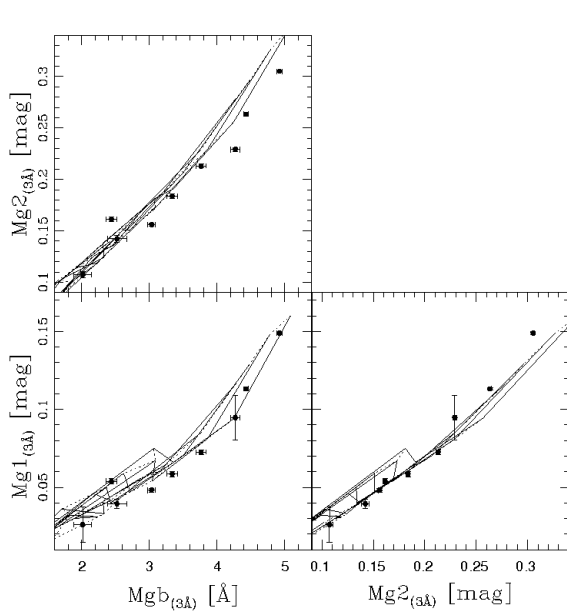


Figure 3. Consistency test using Mg indices and BC03 models at 3 Å resolution. Folded grids are BC03 models and datapoints correspond to central indices (within $R_e/8$) of S0 galaxies in Fornax Cluster.

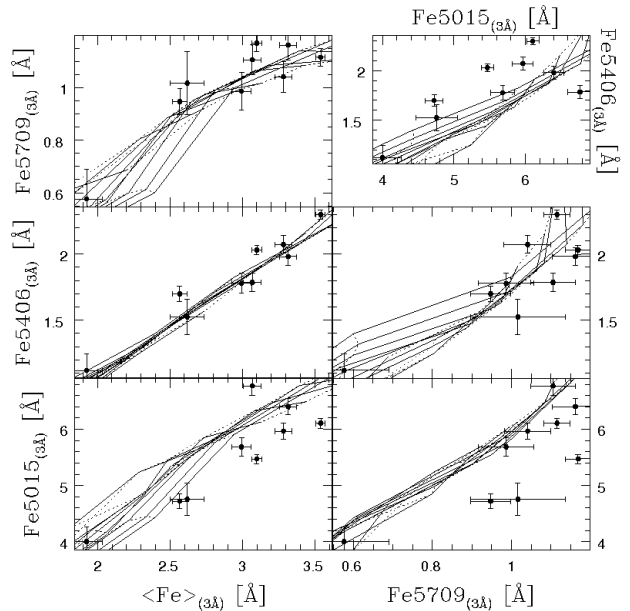


Figure 4. Consistency test using Fe indices and BC03 models at 3 Å resolution. Folded grids are BC03 models and datapoints correspond to central indices (within $R_e/8$) of S0 galaxies in Fornax Cluster.

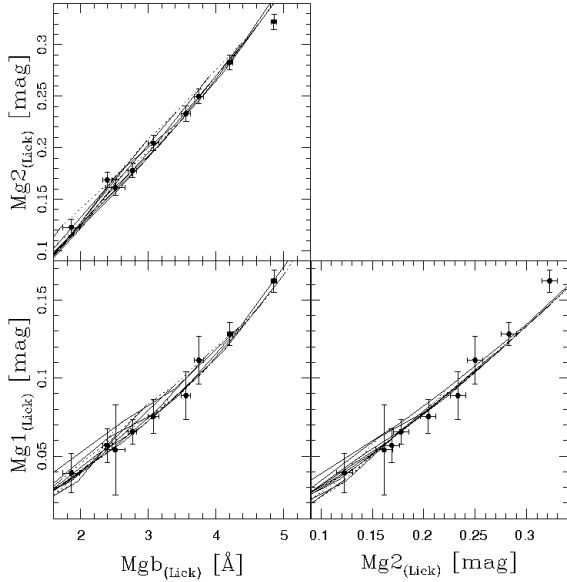


Figure 5. Consistency test using Mg indices and BC03 models at the Lick resolution. Folded grids are BC03 models and datapoints correspond to central indices (within $R_e/8$) of S0 galaxies in the Fornax Cluster.

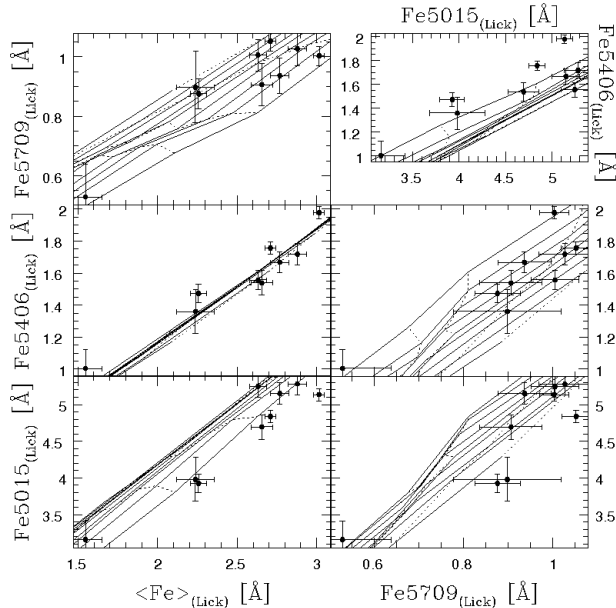


Figure 6. Consistency test using Fe indices and BC03 models at the Lick resolution. Folded grids are BC03 models and datapoints correspond to central indices (within $R_e/8$) of S0 galaxies in the Fornax Cluster.

lowing sections these models can be confidently used to make qualitative comparisons with this data set.

4.2 Lick resolution models and data

The test described in the previous section were also applied to the Lick resolution data and models and the results are presented in Figures 5 and 6.

Figure 6 shows Fe indices in good agreement with model predictions. The scatter found in the previous section and a hint of a systematic deviation in panels involving Fe5015 are also present here, which reinforces the idea that the Fe5015 index must be used with caution. After the spectrophotometric correction applied in section 2.2, a very good match is also found between Mg indices and model grids. In his study of early type galaxies in Fornax, Kuntschner (2000, hereafter K00) found in similar tests discrepancies between the Mg indices and other Lick-based models (Worthey et al. 1994 and Vazdekis et al. 1996). We do not find such differences here. We cannot totally discard, however, the existence of such systematic discrepancies found by K00 given (i) the large uncertainties of our Lick spectrophotometric corrections (derived from a small sample) and (ii) the relatively large errors of our Mg_1 indices.

We cannot discard other sources for the individual offsets between models and data (at both, Lick and 3Å resolutions). For example, the index Mg_1 is highly dependent on the element carbon, which could explain some deviations observed in Figures 3 and 5 if some peculiarities in carbon are present.

In any case, given the good agreement between models and data, and having in mind the discussion in Section 2.1 (see footnote ²), we can confidently use these models to calculate ages and metallicities for individual galaxies.

5 RESULTS AND DISCUSSION

In this section, the main results of the central (within $R_e/8$) stellar populations study are presented. As mentioned earlier, K00 studied the central stellar populations of all ellipticals and S0s in the Fornax Cluster using lower quality optical spectra than the ones presented in this work. Therefore, his study will be a constant reference in the forthcoming pages.

From this point on, the BC03 models at 3Å resolution were always preferred for *qualitative* comparisons between the data and model grids. Also, for the correlations between line indices versus different dynamical mass tracers (e.g. Index*– $\log(\sigma_0)$ relations) the 3Å resolution data were used in order to study the spectral features in grater detail. *Only for the explicit calculation of ages, metallicities and abundances tracers* (e.g. $[\text{Fe}/\text{H}]_{\text{Mgb}} - [\text{Fe}/\text{H}]_{\langle\text{Fe}\rangle}$, $\text{Mgb}/\langle\text{Fe}\rangle$) *were the models and data at the Lick resolution applied.* Unless explicitly mentioned, the 3Å resolution data and models should be assumed.

Following previous works in this field (e.g. K00; Mehlert et al. 2003; Sánchez-Blázquez et al. 2006), we focus our study of central stellar populations on the relations between different line indices and kinematical parameters of the host galaxies. The relations between 10 line indices and the central velocity dispersion, σ_0 , are studied in order to unmask the driving variables behind the observed slopes and scatter. In Figure 7, the relations between line indices and $\log(\sigma_0)$ are presented for the sample of 9 S0s.

Rather than forming continuous trends, Figure 7 shows the three bright galaxies (NGC 1316, 1380 and 1381) and the rest of faint S0s in two separate clumps, each one in opposite extremes of the σ_0 range. However, because the sample was selected only according to morphological classification at optical wavelengths (see K00), there is no obvi-

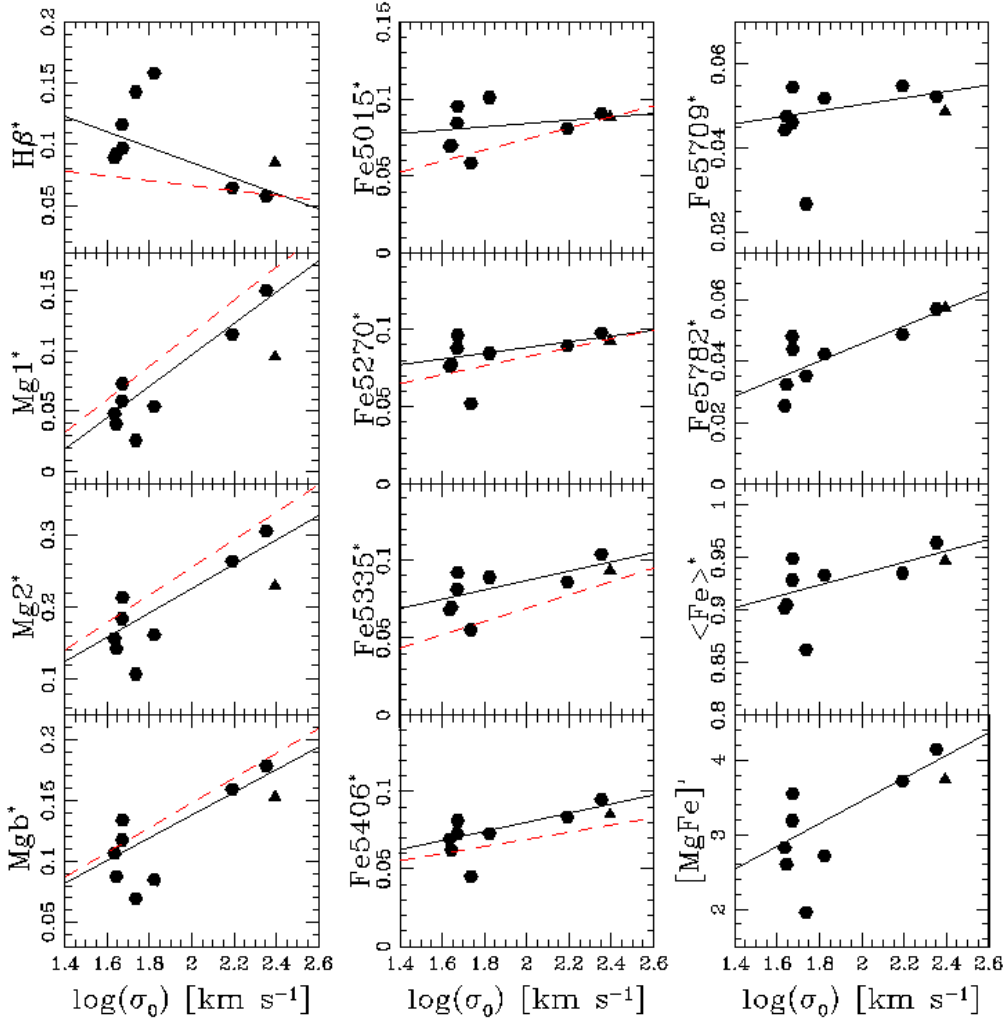


Figure 7. Central line indices (in magnitudes) versus $\log(\sigma_0)$. Continuous lines are the best fits to the datapoints; red dashed lines represent the best fits to normal ellipticals in Fornax from Kuntschner (2000).

ous selection bias against galaxies of intermediate σ_0 values. Therefore, this sample will be considered to describe the two extremes of continuously-populated $\text{Index}^* - \log(\sigma_0)$ relations.

The plots in Figure 7 reconfirm some of the results already indicated by K00. First, faint S0s have a large scatter with respect to the main relations, while the bright galaxies NGC 1380 and NGC 1381 closely follow the relations for ellipticals estimated by K00 (red dashed lines in Figure 7).

Second, the merger remnant NGC 1316 (triangle in Figure 7) departs significantly from the Mg_1 - and Mg_2 - $\log(\sigma_0)$ relations (at more than 4-sigma level in both indices) towards low Mg absorption at a given σ_0 , while closely following the remaining Fe- $\log(\sigma_0)$ relations. These facts, and the comparatively high H β absorption in the H β - $\log(\sigma_0)$ diagram have been interpreted by K00 as the signature of the presence of a younger stellar population in this galaxy, probably formed during the merger. Such a young population could reduce the intensity of some metallic features by increasing the overall continuum level. This effect would

be particularly important for strong metallic features, like the Mg triplet (indices Mgb and Mg_2) and for the molecular indices Mg_1 and Mg_2 whose pseudocontinuum level is strongly dependent on large-scale changes in the continuum. The weaker Fe features in this spectral range could be less influenced by this effect, explaining why NGC 1316 appears in good agreement with the mean Fe relations.

Finally, the slopes of the Mg- $\log(\sigma_0)$ trends are steeper than the ones for the Fe lines (see fit equations in Table 2), as K00 also found for his fits to normal ellipticals.

5.1 The Slopes of the $\text{Index}^* - \log(\sigma_0)$ relations

To study which parameters are driving the observed slopes in the $\text{Index}^* - \log(\sigma_0)$ relations, the models of BC03 were used to parametrise the individual indices as a function of metallicity ($[\text{Fe}/\text{H}]$) and $\log(\text{age})$ such that

$$\text{Index}_{\text{BC03}}^* = A + B \cdot [\text{Fe}/\text{H}] + C \cdot \log(\text{age}[\text{yr}]), \quad (14)$$

Table 2. Parameters of the linear fits $\text{Index}^* = a + b \cdot \log(\sigma_0)$ of the S0 galaxies in Fornax. σ_{std} is the standard deviation about the fit.

Index	$b \pm \delta(b)$	$a \pm \delta(a)$	σ_{std}
$H\beta^*$	-0.0633 ± 0.0031	0.2114 ± 0.0066	0.0360
$\text{Fe}5015^*$	0.0107 ± 0.0021	0.0625 ± 0.0045	0.0219
Mg_1^*	0.1290 ± 0.0016	-0.1618 ± 0.0034	0.0229
Mg_2^*	0.1683 ± 0.0018	-0.1111 ± 0.0038	0.0462
Mgb^*	0.0932 ± 0.0027	-0.0486 ± 0.0056	0.0258
$\text{Fe}5270^*$	0.0185 ± 0.0022	0.0509 ± 0.0045	0.0161
$\text{Fe}5335^*$	0.0303 ± 0.0025	0.0262 ± 0.0052	0.0135
$\text{Fe}5406^*$	0.0293 ± 0.0027	0.0214 ± 0.0056	0.0112
$\text{Fe}5709^*$	0.0077 ± 0.0025	0.0349 ± 0.0053	0.0125
$\text{Fe}5782^*$	0.0284 ± 0.0032	-0.0113 ± 0.0068	0.0071
$\langle \text{Fe} \rangle^*$	0.0538 ± 0.0037	0.8272 ± 0.0077	0.0310
$[\text{MgFe}]'$	1.5212 ± 0.0801	0.4087 ± 0.1661	0.5311

where $\text{Index}_{\text{BC03}}^*$ are index values from BC03 models and

$$B = \frac{\partial(\text{Index}_{\text{BC03}}^*)}{\partial[\text{Fe}/\text{H}]}, \quad (15)$$

$$C = \frac{\partial(\text{Index}_{\text{BC03}}^*)}{\partial(\log(\text{age}))}. \quad (16)$$

Because the galaxies in this sample cover a wide range in ages and $[\text{Fe}/\text{H}]$, we use models with ages from 1.0 to 12.6 Gyr and metallicities from -0.64 to 0.55 dex. The resulting parametrisations are presented in Table 3. The last two columns give the required dependence of $\log(\sigma_0)$ on $[\text{Fe}/\text{H}]$ and age respectively, if that is the *only* driving variable for the observed slopes in the $\text{Index}^* - \log(\sigma_0)$ relations. This dependency was estimated for each index by combining the parametrisations from the models (eqs. 15 and 16) with the slopes measured in Figure 7 (b in Table 2). If $[\text{Fe}/\text{H}]$ is considered as the driver of the observed $\text{Index}^* - \log(\sigma_0)$ trends

$$\frac{b}{B} = \frac{\partial(\text{Index}^*)}{\partial(\log(\sigma_0))} \cdot \frac{\partial[\text{Fe}/\text{H}]}{\partial(\text{Index}_{\text{BC03}}^*)} = \frac{\partial[\text{Fe}/\text{H}]}{\partial(\log(\sigma_0))}. \quad (17)$$

Alternatively, if age is taken as driving variable

$$\frac{b}{C} = \frac{\partial(\text{Index}^*)}{\partial(\log(\sigma_0))} \cdot \frac{\partial(\log(\text{age}))}{\partial(\text{Index}_{\text{BC03}}^*)} = \frac{\partial(\log(\text{age}))}{\partial(\log(\sigma_0))}. \quad (18)$$

Interestingly, these parametrisations show that the $\text{Mg} - \log(\sigma_0)$ relations depend as strongly on age as on metallicity. On the other hand, the slopes of the Fe indices versus $\log(\sigma_0)$ relations can be reproduced with weaker dependencies on metallicity than on age, but the differences between both dependencies are not very large. Naively, a much lower dependence on metallicity relative to the one on age would be expected for these metallicity tracers. Only the behaviour of the $H\beta^* - \log(\sigma_0)$ relation matches the expectations, presenting a slope much easier to reproduce by a small age dependence than by a huge metallicity one.

It is also interesting to note that not all the $[\text{Fe}/\text{H}]$ -sensitive indices have the same dependence on $[\text{Fe}/\text{H}]$; the three Mg indices (Mg_1 , Mg_2 and Mgb) required a stronger $[\text{Fe}/\text{H}]$ dependence than the Fe indices in order to explain their slopes in the $\text{Index}^* - \log(\sigma_0)$ diagrams. This would not be expected if metallicity is the only parameter varying with $\log(\sigma_0)$.

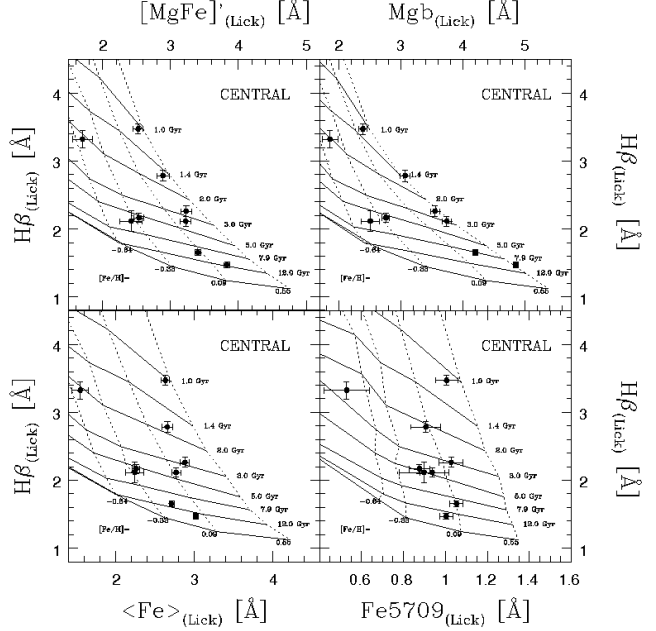


Figure 8. Central metallic indices versus $H\beta$ for S0s in Fornax Cluster. The grids represent BC03 models labeled in terms of age and $[\text{Fe}/\text{H}]$.

Therefore, these results suggest that age could be an important driver of the observed correlations while the role of metallicity is more uncertain. Also a third variable, such as the relative Mg abundances, may affect the relations by producing relative differences between indices, each one with different sensitivities to changes in the chemical composition of these systems (Vazdekis et al. 2001; Sánchez-Blázquez et al. 2006).

5.1.1 The $[\text{Fe}/\text{H}]$ - and $\log(\text{age}) - \log(\sigma_0)$ relations

A closer comparison between the data and the BC03 models could shed more light on the origin of the observed correlations. Individual ages and $[\text{Fe}/\text{H}]$ were calculated by plotting different $[\text{Fe}/\text{H}]$ -sensitive indices versus $H\beta$; *data and models at the Lick resolution were used in this step.* The details of the procedure applied here are described in Cardiel et al. (2003). Briefly, the ages and metallicities were logarithmically-interpolated from the model grid values by fitting the four closest cells to a datapoint with quadratic polynomials. The procedure also considers the effect of covariance when estimating the uncertainties for both parameters. In this way the age- $[\text{Fe}/\text{H}]$ degeneracy is broken and luminosity-weighted estimates of both parameters were obtained. As an example, in Figure 8 four of these plots are presented for the central index values, also including the BC03 model grids labeled in terms of age and $[\text{Fe}/\text{H}]$. Central ages and metallicities for different indices are presented in Table A3 for all the Fornax sample.

In Figure 9, $\log(\sigma_0)$ is plotted against age and $[\text{Fe}/\text{H}]$ using different $[\text{Fe}/\text{H}]$ sensitive indices. The continuous lines represent the best linear fits whose slopes are presented in Table 4. It is surprising that no obvious trends are ob-

Table 3. Parametrisation of the line indices using BC03 models: $\text{Index}_{\text{BC03}}^* = A + B \cdot [\text{Fe}/\text{H}] + C \cdot \log(\text{age}[\text{yr}])$. Last two columns: dependence of $\log(\sigma_0)$ on metallicity (age) if this is the *only* driving variable for the observed slopes in the $\text{Index}^* - \log(\sigma_0)$ relations.

Index	A	$B \pm \delta(B)$	$C \pm \delta(C)$	$\frac{\partial[\text{Fe}/\text{H}]}{\partial(\log(\sigma_0))}$	$\frac{\partial(\log(\text{age}))}{\partial(\log(\sigma_0))}$
$\text{H}\beta^*$	0.7778	-0.0157 ± 0.0014	-0.0712 ± 0.0020	4.029	0.888
Fe5015^*	-0.0854	0.0323 ± 0.0007	0.0177 ± 0.0011	0.330	0.601
Mg_1^*	-0.4602	0.0502 ± 0.0023	0.0547 ± 0.0032	2.568	2.357
Mg_2^*	-0.8310	0.1075 ± 0.0031	0.1053 ± 0.0044	1.564	1.597
Mgb^*	-0.4431	0.0521 ± 0.0014	0.0572 ± 0.0019	1.790	1.629
Fe5270^*	-0.1509	0.0366 ± 0.0005	0.0244 ± 0.0007	0.505	0.757
Fe5335^*	-0.1665	0.0388 ± 0.0006	0.0256 ± 0.0008	0.779	1.180
Fe5406^*	-0.2017	0.0419 ± 0.0006	0.0284 ± 0.0008	0.699	1.029
Fe5709^*	-0.0511	0.0199 ± 0.0007	0.0098 ± 0.0009	0.386	0.781
Fe5782^*	-0.0856	0.0293 ± 0.0006	0.0137 ± 0.0009	0.968	2.074

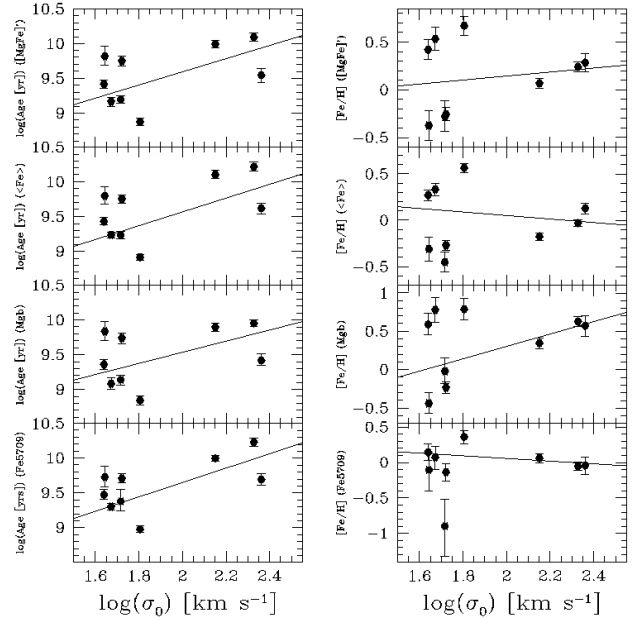
Table 4. Slopes from linear parametrisation of $\log(\text{age})$ or $[\text{Fe}/\text{H}]$ versus $\log(\sigma_0)$ for S0 galaxies in Fornax (Figure 9) using different line indices as metallicity tracers.

Parameter	Slope	Parameter	Slope
$\log(\text{age})_{[\text{MgFe}]'}$	0.946 ± 0.079	$[\text{Fe}/\text{H}]_{[\text{MgFe}]'}$	0.208 ± 0.090
$\log(\text{age})_{\langle \text{Fe} \rangle}$	0.994 ± 0.075	$[\text{Fe}/\text{H}]_{\langle \text{Fe} \rangle}$	-0.189 ± 0.057
$\log(\text{age})_{\text{Mgb}}$	0.803 ± 0.080	$[\text{Fe}/\text{H}]_{\text{Mgb}}$	0.806 ± 0.106
$\log(\text{age})_{\text{Fe5709}}$	1.033 ± 0.074	$[\text{Fe}/\text{H}]_{\text{Fe5709}}$	-0.189 ± 0.113

served in any of the $[\text{Fe}/\text{H}] - \log(\sigma_0)$ plots, considering that the $\text{Index} - \log(\sigma_0)$ relations are usually attributed, at least for ellipticals, to a chemical composition change with galaxy mass. The slope for the $[\text{Fe}/\text{H}] - \log(\sigma_0)$ relation using Mgb seems to be an artifact of the linear fit instead of pointing to a real correlation. Comparing the slopes for metallicity presented in Table 4 with the required metallicity dependences for each $\text{Index}^* - \log(\sigma_0)$ relation in Table 3 it is clear that $[\text{Fe}/\text{H}]$ cannot be the main driver of any of the Index^* correlations with $\log(\sigma_0)$. The plots against age present stronger trends in the same direction as the $\text{Index}^* - \log(\sigma_0)$ diagrams: the three high-dispersion galaxies seem to be, on average, older than the rest of the sample. This result holds for all the age estimations, including the one using $[\text{MgFe}]'$ which is insensitive to α -element relative abundance variations. Comparing the slopes of these relations with the required age dependences for the observed $\text{Index}^* - \log(\sigma_0)$ trends, we found that the $\text{H}\beta^*$ and almost all the Fe trends can be explained by an age effect. However, differences in relative age do not seem to explain the steeper slopes found for the Mg indices in comparison to Fe, reinforcing the idea that α -element relative abundances are playing an important role too.

5.1.2 The $[\text{Mg}/\text{Fe}] - \log(\sigma_0)$ relations

At the beginning of this section, the possibility of a Mg (or α -element) abundance dependence of the $\text{Index}^* - \log(\sigma_0)$ relations was suggested, and this possibility was re-enforced by the results presented above. This alternative was further explored by plotting Mg-sensitive versus Fe-sensitive indices and comparing the data to the solar-abundance predictions of the models (see Worthey, Faber & Gonzalez 1992). In Figure 10, twelve panels plotting central Mg versus Fe indices are presented, together with BC03 model grids. What

**Figure 9.** Central Ages and metallicities versus $\log(\sigma_0)$ for Fornax S0s. Lines represent the best linear fits to the data.

is clear from almost all these panels is that the three highest-dispersion galaxies in the sample (open symbols in Figure 10) are not accurately described by models that assume solar abundance ratios, presenting stronger Mg indices for a given Fe index than the model predictions. Among these three galaxies, the effect seems to be stronger for NGC 1380 and 1381, while NGC 1316 (the merger remnant) is usually closer to the solar-model grids. In similar plots, K00 found that only the nucleus of NGC 1380 presented this behaviour, suggesting that this galaxy is Mg overabundant compared to Fe.

In order to trace the relative Mg overabundances we compare the relative metallicities derived from Fe- and Mg-sensitive indices and the same age indicator ($\text{H}\beta$ in this case). At this point, it is worthy to stress that we are not attempting to derive absolute Mg (or α -elements) abundances. By comparing different metallicity estimates (and by using $\text{Mgb}/\langle \text{Fe} \rangle$, see below) we aim to *trace* the *relative* Mg abun-

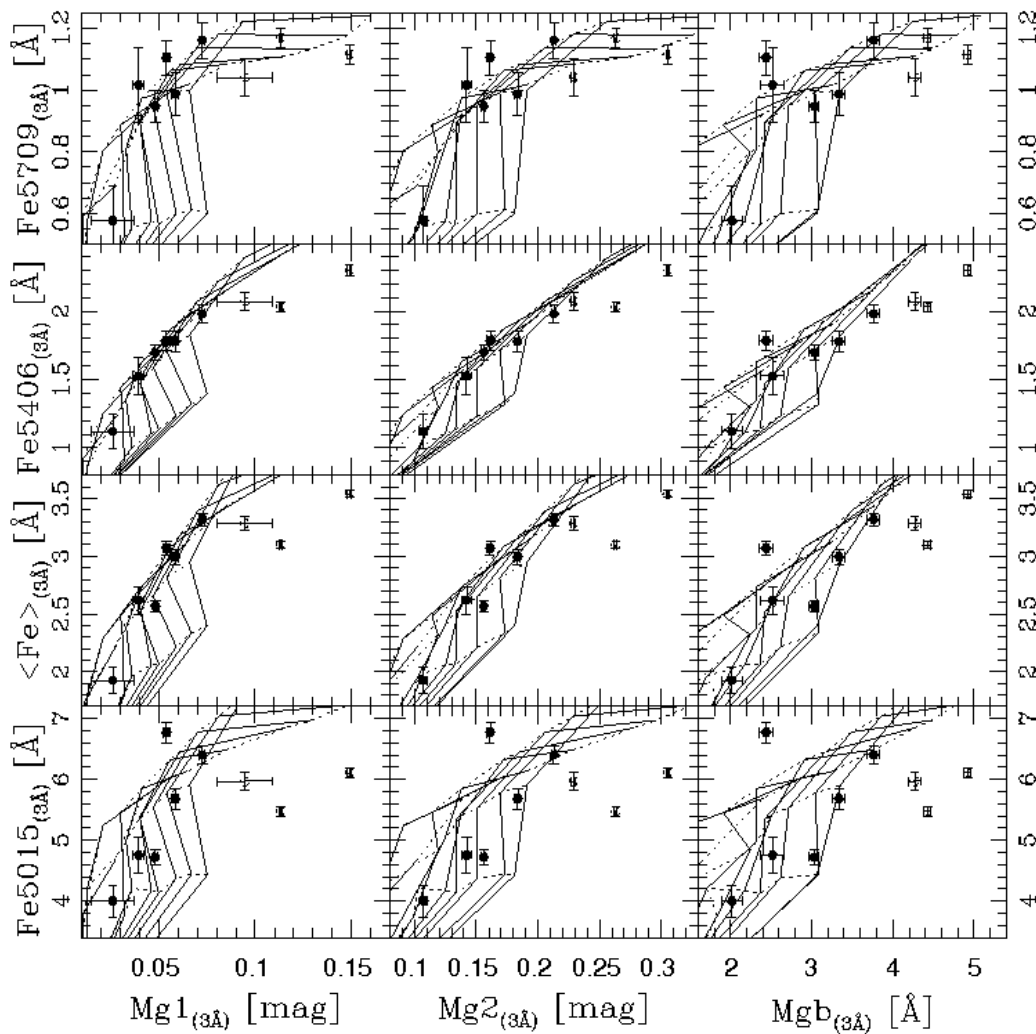


Figure 10. Central Mg versus Fe indices for Fornax S0s. Grids correspond to BC03 models at 3 Å resolution.

dances. All our results and conclusions are independent of absolute abundance ratios.

In the top panel of Figure 11, $\log(\sigma_0)$ is plotted against the difference of the metallicities calculated by using Mgb and $\langle Fe \rangle$ as metallicity indicators. Data and models at the Lick resolution were used to estimate these metallicities. It is apparent from this plot that bright S0s are, on average, Mg overabundant relative to fainter galaxies; however the uncertainties coming from the models make this difference only marginally significant. The bottom panel of Figure 11 shows the index quotient $Mgb/\langle Fe \rangle$ versus the velocity dispersion. The ratio of these two indices has been used by TMB03 to calibrate the $[\alpha/Fe]$ abundance ratio of their models, so it traces the relative behaviour of the Mg overabundance and, equally important, it provides a model-independent test. With much reduced errors, it is clear that bright S0s have larger $Mgb/\langle Fe \rangle$ ratios than fainter objects. This model-independent test can explain why the slopes of the $\text{Index}^* - \log(\sigma_0)$ correlations are steeper for the Mg indices than for the Fe ones, confirming the previous results

of this section. The overall results also imply the existence of a correlation between age and $Mgb/\langle Fe \rangle$ (or $[\alpha/Fe]$; see Figure 17, bottom panel in first column), in agreement to the previous findings of Fisher, Franx & Illingworth (1995) and Thomas, Maraston & Bender (2002) in elliptical galaxies.

Different authors have tried to explain the observed $[Mg/Fe]$ overabundances in the context of galaxy formation and evolution. All these scenarios are based on nucleosynthesis models which predict that Type II supernovae mainly eject α -elements, like Mg, while Type Ia supernovae are the main sources of enrichment of the ISM with Fe. Possible explanations include variations in the initial mass function (e.g. Schmidt 1963; Worthey et al. 1992; Vazdekis et al. 1999; Nagashima et al. 2005), selective loss of metals (Worthey et al. 1992), different time scales of star formation and different star formation histories. The last two have been very popular in the last few years in order to explain the observed overabundances in bright ellipticals (e.g. Mehlert et al. 2003; Sánchez-Blázquez et al. 2006). In this scenario, early-type galaxies are believed to be remnants of gaseous mergers.

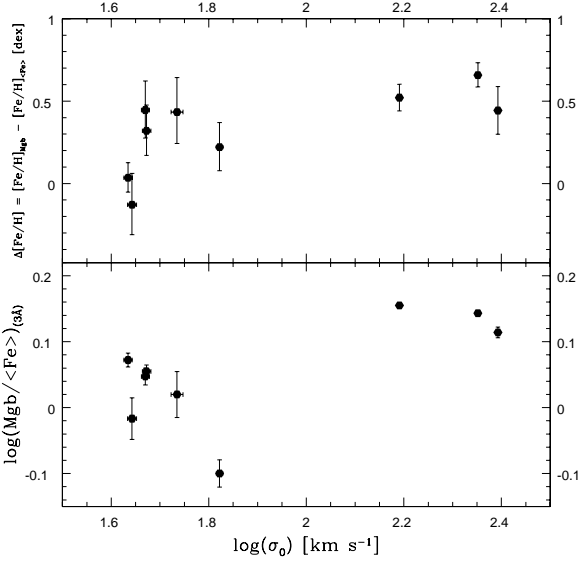


Figure 11. Mg/Fe relative abundance tracers versus $\log(\sigma_0)$ for Fornax S0s.

This process produces a starburst where part of the gas is consumed and the remainder is ejected via stellar winds (for low mass remnants) or heated by different mechanisms (e.g. AGN, SNe, thermal conduction) in more massive systems, stopping further star formation. According to the hierarchical merging paradigm, the starburst is more intense in the central regions of the remnant given the stronger potential well in the centre and subsequent dissipation of the gas towards it. The merger process implies a faster build-up of the system total mass, having shorter star formation timescales than systems grown by secular or more gentle processes. A short burst of star formation would not give enough time to incorporate the gas enriched with Fe from SNe Type Ia to the formation of further generations of stars, while SNe Type II would succeed in incorporation α -elements (like Mg) given their much quicker occurrence (in less than 1 Gyr). In consequence, a relative [Mg/Fe] overabundance will be observed in these systems (understood as an *underabundance* of Fe) with respect to galaxies with younger luminosity-weighted ages and more extended star formation histories.

This scenario is in agreement with the results found here for the bright S0s, and is not surprising for NGC 1316, a well known merger remnant. However, whether this picture can be applied to the entire NGC 1380 and NGC 1381 galaxies or only to their nuclei, is something that cannot be tested with central line indices alone.

5.1.3 The Residuals of the $\text{Index}^* - \log(\sigma_0)$ relations

Previous studies have looked for correlations between the $\text{Index}^* - \log(\sigma_0)$ residuals (ΔIndex^*) and different parameters that characterise the galaxies' structure or their stellar populations. Some of these efforts point out the existence of a dependence between ΔIndex^* and the relative ages of elliptical galaxies (Schweizer et al. 1990; González & Gorgas 1996; Worthey & Collobert 2003) by comparing the residuals to the index $H\beta$. Hints of similar trends are seen for the

Table 5. Parameters of linear fits $\text{Index}^* = a + b \cdot \log(V_{\text{MAX}})$ of S0 galaxies in Fornax. σ_{std} is the standard deviation about the fit.

Index	$b \pm \delta(b)$	$a \pm \delta(a)$	σ_{std}
$H\beta^*$	-0.1099 ± 0.0046	0.3354 ± 0.0108	0.0214
Fe5015*	0.0197 ± 0.0030	0.0389 ± 0.0071	0.0143
Mg ₁ *	0.2015 ± 0.0026	-0.3665 ± 0.0062	0.0233
Mg ₂ *	0.2593 ± 0.0026	-0.3633 ± 0.0061	0.0355
Mgb*	0.1446 ± 0.0038	-0.1906 ± 0.0089	0.0194
Fe5270*	0.0358 ± 0.0031	0.0062 ± 0.0073	0.0070
Fe5335*	0.0462 ± 0.0036	-0.0181 ± 0.0083	0.0094
Fe5406*	0.0475 ± 0.0038	-0.0279 ± 0.0090	0.0057
Fe5709*	0.0185 ± 0.0037	0.0080 ± 0.0086	0.0050
Fe5782*	0.0377 ± 0.0047	-0.0399 ± 0.0109	0.0098
$\langle\text{Fe}\rangle^*$	0.0895 ± 0.0053	0.7313 ± 0.0122	0.0166
$[\text{MgFe}]'$	2.5019 ± 0.1147	-2.2356 ± 0.2655	0.2802

Mg indices of these S0 galaxies but they do not seem to be statistically significant, while residuals from the Fe relations are clearly uncorrelated with $H\beta$. Potential correlations between ΔIndex^* and other parameters were explored, including kinematical (σ_0 ; maximum -circular- rotational velocity, V_{MAX}) and structural (R_e , R_d , bulge-to-total fraction, Sérsic index) parameters derived in Papers I and II. No statistically significant trends were found for any of these combinations.

5.2 The $\text{Index}^* - \log(V_{\text{MAX}})$ relations and the Dynamical Mass

Given the strong rotational support of many of these S0 galaxies, we decided to explore the $\text{Index}^* - \log(V_{\text{MAX}})$ relations. Figure 12 shows the different line indices versus maximum (circular) rotational velocity, where clear trends appear in all the panels. Linear least-squares fits to the data were performed and presented as straight lines in each panel. The galaxy with the lowest velocity, ESO 359-G002, was excluded from the fitting process because the slope and zero-points would be strongly affected by this pressure-supported object for which V_{MAX} is highly uncertain. The exclusion of the other pressure-supported galaxy, NGC 1316, does not significantly affect the fitted slopes and zero-points.

In Table 5 the linear fit coefficients and standard deviations, σ_{std} , are presented. It is interesting to notice that for almost all the indices, σ_{std} is smaller than its counterpart from the $\text{Index}^* - \log(\sigma_0)$ fits (see Table 2). If we assume that mass is the fundamental physical parameter governing the properties of these galaxies, the improvement in the fits may be interpreted in the sense that V_{MAX} is a better estimator of the total dynamical mass than σ_0 , which is not totally surprising after highlighting in Paper I the predominant rotational nature of these systems. As a test, the mass of these galaxies was parametrised as a function of the velocity dispersion and of V_{MAX} in order to compare how central indices correlate with both possible descriptions. If the galaxies are supported by rotation, we can write

$$M \propto V_{\text{MAX}}^2 \cdot R_d, \quad (19)$$

where M is the total dynamical mass and the disk scale-length, R_d , was used to characterise the radius of the galaxies because it reaches the regions where the rotation curves

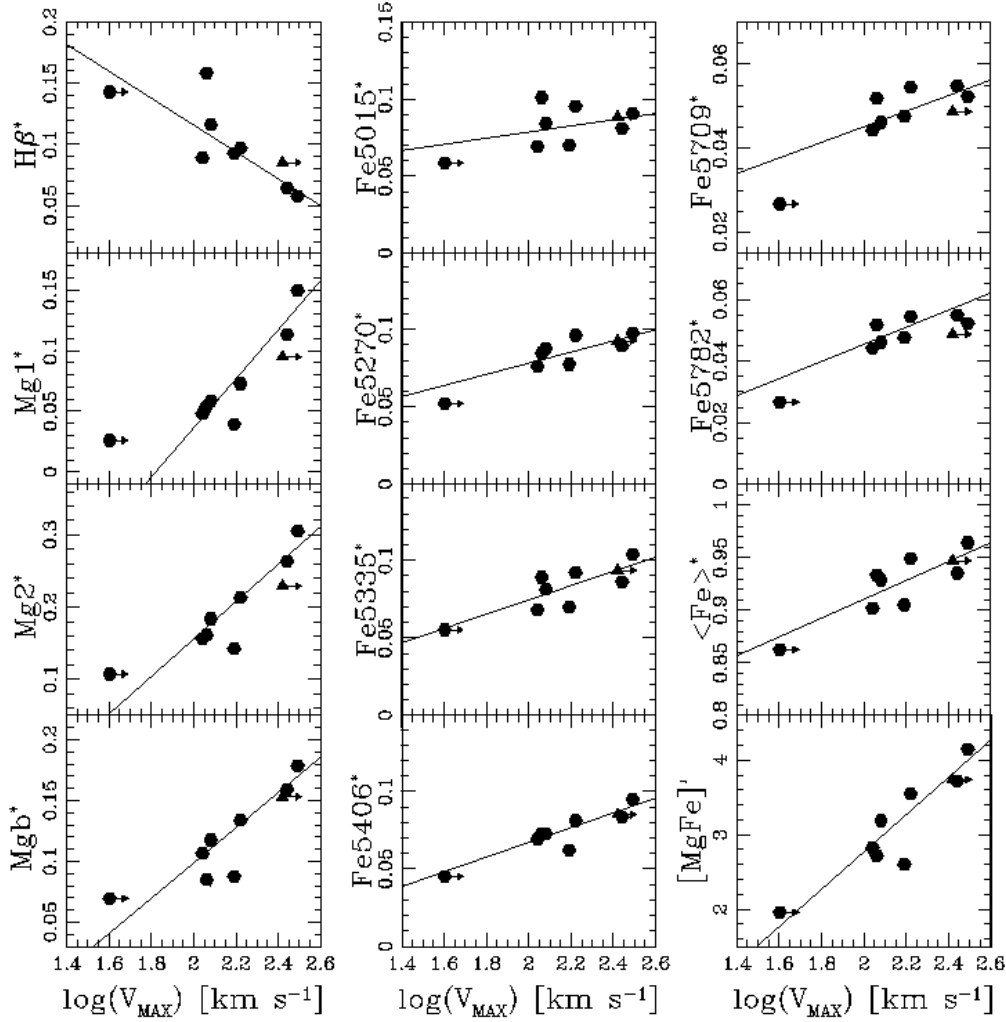


Figure 12. Central line indices (in magnitudes) versus $\log(V_{\text{MAX}})$. Solid lines are the best fits to the datapoints, excluding ESO 359-G002. The triangle represents NGC 1316, a merger remnant. For the two galaxies with arrows, the deprojected azimuthal velocity, V_ϕ , was used instead of V_{MAX} as a lower limit.

become flat. If the galaxies are mainly supported by velocity dispersion, a similar expression can be obtained,

$$M \propto \langle \sigma^2 \rangle_{R_e} \cdot R_e, \quad (20)$$

where R_e is the effective radius of the bulge and $\langle \sigma^2 \rangle_{R_e}$ is the average mean-square dispersion inside R_e . Other measures of scale such as the half-light radius determined in Paper 2 produce similar results, but for this analysis R_e is adopted because it is well constrained by the GIM2D models (Simard et al. 2002).

In Figures 13 and 14, central line indices are plotted versus $R_e \cdot \langle \sigma^2 \rangle_{R_e}$ and $R_d \cdot V_{\text{MAX}}^2$, respectively. Clearly, both parameters, σ and V_{MAX} , are tracing, to some extent, the mass of these systems. However, an important difference arises between pressure- and rotation-supported galaxies (open and filled dots, respectively): when the mass is estimated using σ , it is underestimated in rotationally supported systems with respect to pressure-supported ones, as it is evident from the

offset between open and filled dots in Figure 13. On the other hand, Figure 14 shows that if we estimate the mass using V_{MAX} , all the galaxies follow a common sequence. In this plot, lower limits for the two pressure-supported S0s (using V_ϕ) are indicated as open dots with arrows. For these two galaxies, masses were also estimated from their measured σ 's by assuming a simple isothermal sphere in hydrostatic equilibrium and presented as open stars in Figure 14. The much tighter trends observed in this plot are consistent with our hypothesis that V_{MAX} is a much better tracer of the dynamical mass of these systems than σ .

Figure 15 presents central ages and $[\text{Fe}/\text{H}]$ from BC03 models and $\text{Mgb}/\langle \text{Fe} \rangle$ versus 3 different dynamical mass tracers (V_{MAX} , $R_e \cdot \langle \sigma^2 \rangle_{R_e}$ and $R_d \cdot V_{\text{MAX}}^2$). No strong correlations are obvious from the central stellar population properties plotted against the dynamical mass. However, for $R_d \cdot V_{\text{MAX}}^2$ mass tracer, a Spearman rank and a Student-t correlation tests (Table 6) indicate that the relation between

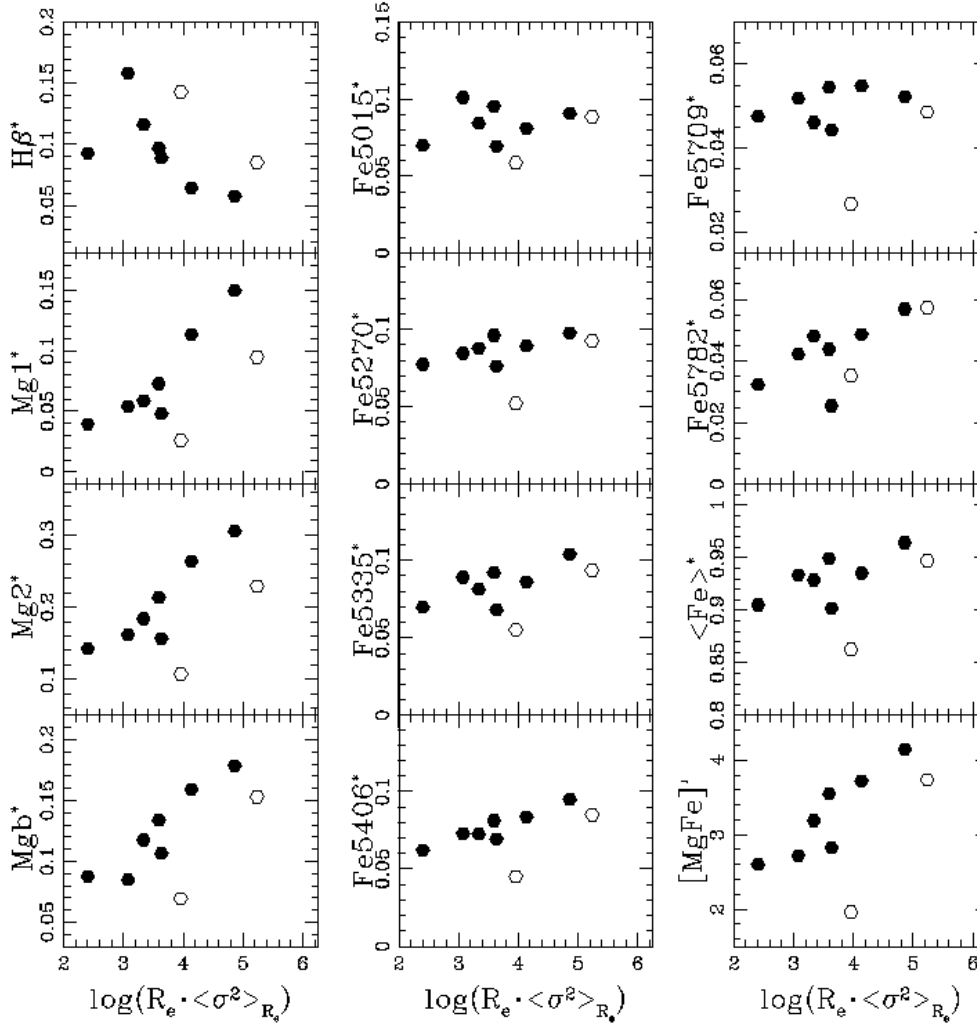


Figure 13. Central line indices versus $\log(R_e \cdot \sigma_{(R_e)}^2)$, proportional to the total dynamical mass for pressure-supported galaxies. Open symbols represent NGC 1316 and ESO 359-G002, two pressure supported galaxies.

the $[\alpha/\text{Fe}]$ tracer and dynamical mass is significant at a 95–99% confidence level. To understand the absence of other correlations, we explore the possibility that the uncertainties in BC03 models are washing out the real trends with age and metallicity by considering other SSP models. We have used an improved version of Vazdekis et al. (1996) models (Vazdekis et al. in preparation; hereafter Vaz96) and recalculate all central ages and metallicities ($[\text{M}/\text{H}]$ in Vaz96 nomenclature) for our S0 sample³. In Figure 16, we present the resulting ages and $[\text{M}/\text{H}]$ versus different mass tracers. No strong correlations are observed either with the new model predictions, weakening the assumption that model artifacts are responsible of the absence of trends between the stellar population parameters and the dynamical mass. An alternative explanation is that the tight correlations ob-

served between the line indices and galaxy mass are not governed by the variation of one of these stellar population parameters alone, but by a combination of them in some correlated way.

Indeed, Figure 17 suggests that age and α -element overabundance are correlated (97.5% confidence level). High α -element overabundance implies short star-formation timescale. This can be understood by considering a simple model for the star-formation history of the Fornax S0s in which all these galaxies started forming stars at approximately the same time and formed stars for a period Δt . Thereafter, star formation ceased and the galaxies evolved passively for a time t until the epoch of observation. The age derived from the absorption-line indices is $\simeq t$, while the α -element overabundance is anticorrelated with Δt . In this simple model t is anticorrelated with Δt , and it follows that the measured age must be correlated with the α -element overabundance, as observed. If this interpretation is correct, the most massive S0s have the shortest star-formation

³ We have used $\text{H}\beta$ and $[\text{MgFe}]'$ indices at Lick resolution as our age and metallicity indicators, respectively.

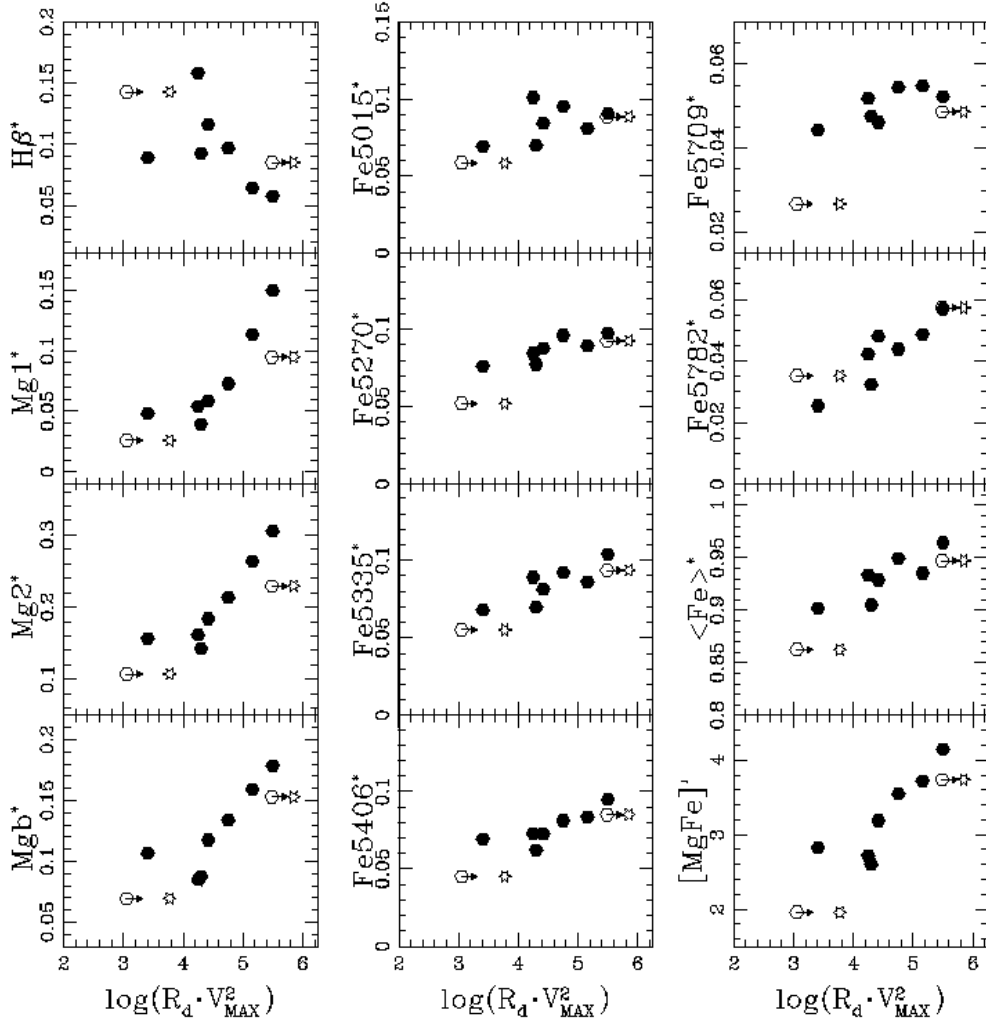


Figure 14. Central line indices versus $\log(R_d \cdot V_{\text{MAX}}^2)$, proportional to the total dynamical mass for rotationally-supported galaxies. Open symbols with arrows represent NGC 1316 and ESO 359-G002, two pressure supported galaxies. For these two objects the deprojected azimuthal velocity, V_ϕ , was used as a lower limit instead of V_{MAX} . Open stars correspond to the dynamical mass of these two galaxies estimated from σ by assuming an isothermal sphere in hydrostatic equilibrium.

Table 6. Spearman and Student-t tests for central stellar population parameters versus dynamical mass of S0 galaxies in Fornax (as estimated from $R_d \cdot V_{\text{MAX}}^2$, third column in Figure 15). In parenthesis, probability of rejecting the null hypothesis of no correlation.

Dyn. Mass vs.	Spearman Test Coeff.	Student-t test Coeff.
$\log(\text{age})_{[\text{MgFe}]'}$	0.4167 (< 90%)	1.2127 (85–90%)
$[\text{Fe}/\text{H}]_{[\text{MgFe}]'}$	0.2833 (< 90%)	0.7817 (75–80%)
$\text{Mgb}/\langle\text{Fe}\rangle$	0.6833 (95–97.5%)	2.4762 (97.5–99%)

timescales (cf. §5.1.2) and the oldest stellar populations. Obviously, this is an oversimplified model, but it explains, at least qualitatively, the observed trends.

6 CONCLUSIONS

This paper presents the study of a sample of 9 S0 galaxies in the Fornax Cluster previously described in Paper I. By linking the properties of the central stellar populations (ages, chemical abundances) of these galaxies and their global properties (mass and dynamics), we uncover important clues on the main physical drivers governing the formation and evolution of S0s. Our main conclusions are the following:

- Central absorption line indices correlate with central velocity dispersions in a way similar to what previous studies found for elliptical galaxies. However, a study of the stellar population properties of the Fornax S0s reveals that the trends shown by their line indices seem to be produced by relative differences in age and α -element abundances, contrary to what is found in ellipticals where the overall metallicities are important drivers of the correlations.

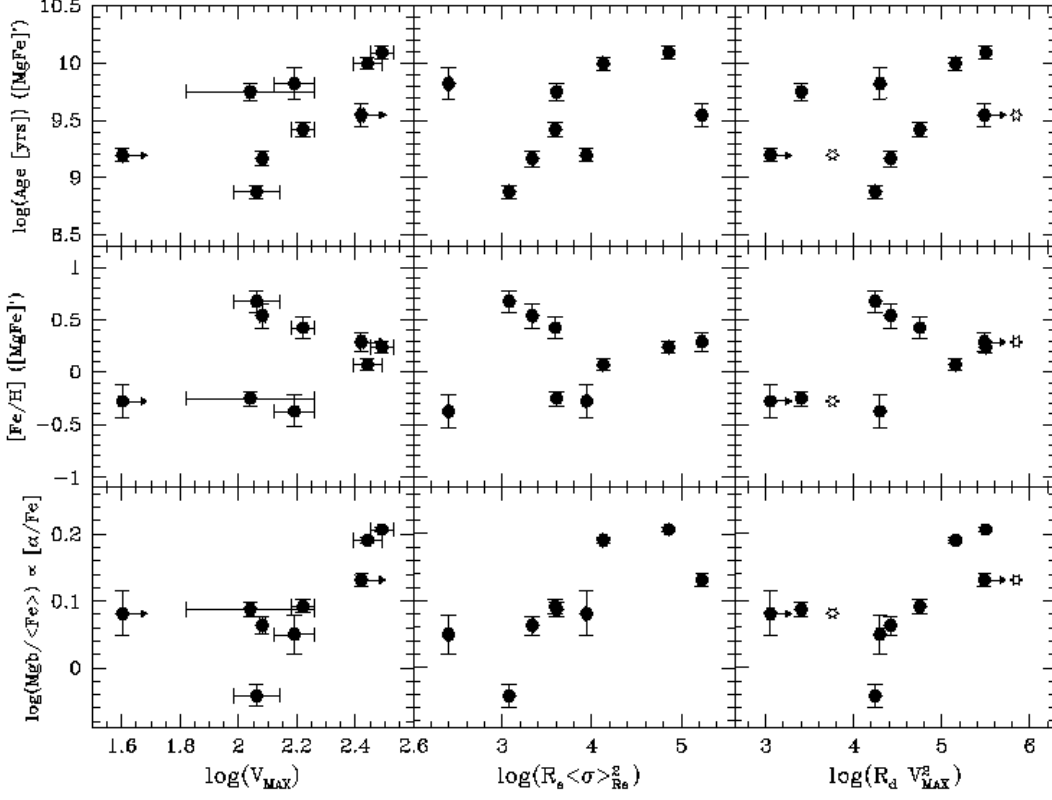


Figure 15. Central ages and metallicities from BC03 models and $\text{Mgb}/\langle\text{Fe}\rangle$ ($\propto \alpha$ -elements overabundance) versus 3 different dynamical mass tracers. The same symbols are used as in Figure 14.

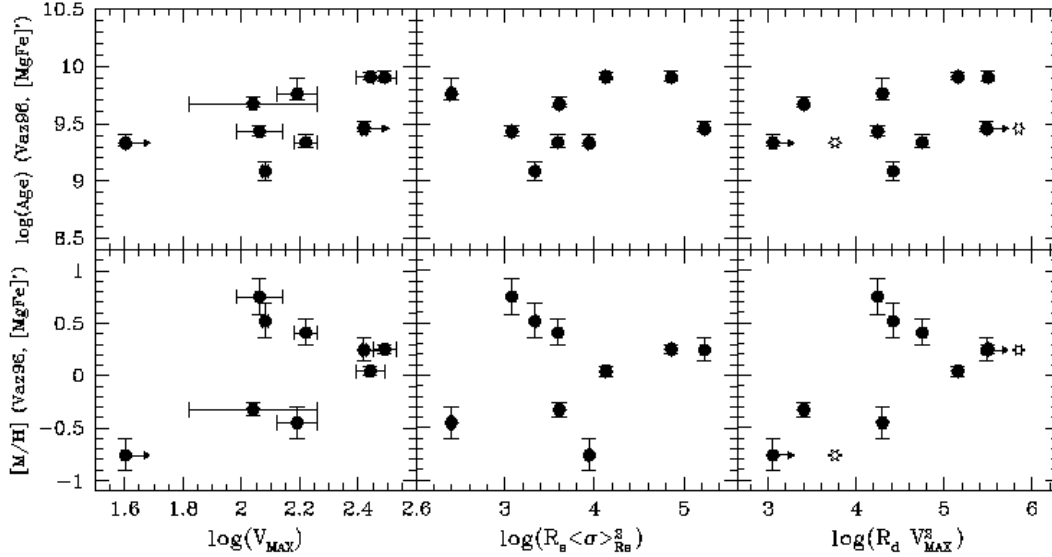


Figure 16. Central ages and metallicities from an improved version of Vaz96 models (Vazdekis et al. in preparation) versus 3 different dynamical mass tracers. The same symbols are used as in Figure 14.

- The scatter in the $\text{Index}^* - \log(\sigma_0)$ relations can be partially explained by the rotationally-supported nature of many S0s. The tighter correlations found between Index^* and $\log(V_{\text{MAX}})$ support this interpretation.
- The dynamical mass seems to be the primary physi-

cal property governing these correlations and in the Fornax S0s we need to study it by considering their rotationally-supported nature. For these systems, V_{MAX} is a better tracer of dynamical mass than σ .

- The α -element overabundance of these galaxies seems

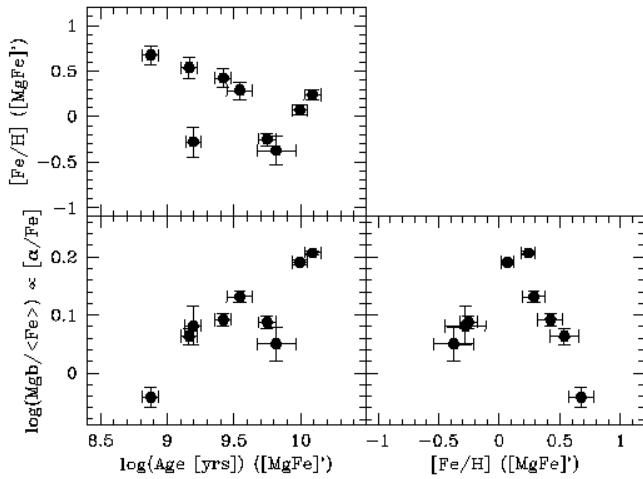


Figure 17. Central ages and metallicities from BC03 models and $Mgb/\langle Fe \rangle \propto [\alpha\text{-elements overabundance}]$ versus each other.

to be correlated with their mass. Moreover, the absorption-line-derived ages also correlate with the overabundances. This implies that the most massive S0s have the shortest star-formation timescales and the oldest stellar populations.

These results support the idea of different star formation histories for the central regions of bright and faint S0 galaxies. Other authors have reached similar conclusions by studying early-type systems in the Coma Cluster (Poggianti et al. 2001; Mehlert et al. 2003).

The results found here are consistent with a scenario where faint S0s are descendants of spiral galaxies who lost (or exhausted) their gas and suffered a final central gasp of star formation during cluster infall, while bright systems seem to have star formation histories resembling those of normal ellipticals. However, are the nuclei characterising the entire galaxies? Have the outermost regions another story to tell? These questions lie beyond the scope of this study, but will be addressed in the following paper of the series, when a stellar population study at larger galactocentric distances will give us new clues about the detailed star formation history of S0s in the Fornax Cluster.

ACKNOWLEDGMENTS

This work was based on observations made with ESO telescopes at Paranal Observatory under programme ID 070.A-0332. This publication makes use of data products from the Two Micron All Sky Survey, which is a joint project of the University of Massachusetts and the Infrared Processing and Analysis Center/California Institute of Technology, funded by the National Aeronautics and Space Administration and the National Science Foundation.

References

Aragón-Salamanca A., Bedregal A.G., Merrifield M.R., 2006, *A&A*, 458, 101
 Bedregal A.G., Aragón-Salamanca A., Merrifield M.R., Milvang-Jensen B., 2006a, *MNRAS*, 371, 1912 (Paper I)

Bedregal A.G., Aragón-Salamanca A., Merrifield M.R., 2006b, *MNRAS*, 373, 1125 (Paper II)
 Bender R., Burstein D., Faber S.M., 1993, *ApJ*, 411, 153
 Bernardi M., Renzini A., da Costa L.N., Wegner G., Alonso M.V., Pellegrini P.S., Rit  C., Willmer C.N.A., 1998, *ApJ*, 508, 143
 Bruzual G., Charlot S., 2003, *MNRAS*, 244, 1000B
 Burstein D., Faber S.M., Gaskell C.M., Krumm N., 1984, *ApJ*, 287, 586
 Burstein D., Davies R.L., Dressler A., Faber S.M., Lynden-Bell A., Terlevich R.J., Wegner G., 1988, in *Towards Understanding Galaxies at Large Redshifts*, Ed: R.G. Kron and A. Renzini, (Kluwer, Dordrecht), 17
 Caldwell N., 1984, *PASP*, 96, 287
 Cardiel N., Gorgas J., Cenarro J., Gon lez J.J., 1998, *A&AS*, 127, 597
 Cardiel N., Gorgas J., S nchez-Bl zquez P., Cenarro A.J., Pedraz S., Bruzual G., Klement J., 2003, *A&A*, 409, 511
 Colless M., Burstein D., Davies R.L., McMahan R.K., Saglia R.P., Wegner G., 1999, *MNRAS*, 303, 813
 Fisher D., Franx M., Illingworth G.D., 1995, *ApJ*, 448, 119
 Gallazzi A., Charlot S., Brinchmann J., White S.D.M., 2006, *MNRAS*, 370, 1106
 Gon lez J.J., 1993, PhD Thesis, University of California, Santa Cruz
 Gon lez J.J., Gorgas J., 1996, in *Fresh views of elliptical galaxies*, ed. A. Buzzoni, A. Renzini, ASP Conf. Ser., 86, 225
 Gorgas J., Efstathiou G., Arag n-Salamanca A., 1990, *MNRAS*, 245, 217
 Goudfrooij P., Hansen L., Jorgensen H.E., Norgaard-Nielsen H.U., 1994, *A&AS*, 105, 341
 Guzm n R., Lucey J.R., Carter D., Terlevich R.J., 1992, *MNRAS*, 257, 187
 Jorgensen I., Franx M., Hjorth J., van Dokkum P.G., 1999, *MNRAS*, 308, 833
 Kuntschner H., 2000, *MNRAS*, 315, 184
 Kuntschner H., Lucey J.R., Smith R.J., Hudson M.J., Davies R.L., 2001, *MNRAS*, 323, 615
 Le Borgne, J. et al. 2003, *A&A*, 402, 433
 Mehlert D., Thomas D., Saglia R.P., Bender R., Wegner G., 2003, *A&A*, 407, 423
 Nagashima M., Lacey C.G., Okamoto T., Carlton M.B., Frenk C.S., Cole S., 2005, *MNRAS*, 363, L31
 Poggianti B. et al. 2001, *ApJ* 563, 118
 Phillips M.M., Jenkins C.R., Dopita M.A., Sadler E.M., Binette L., 1986, *AJ*, 91, 1062
 S nchez-Bl zquez P., 2004, Ph.D. Thesis, Universidad Complutense de Madrid
 S nchez-Bl zquez P., et al., 2006, *MNRAS*, 371, 703
 Schmidt M., 1963, *ApJ*, 137, 758
 Schweizer F., Seitzer P., Faber S.M., Burstein D., Dalle Ore C.M., Gonzalez J.J., 1990, *ApJ*, 364, 33
 Simard L. et al. 2002, *ApJS*, 142, 1S
 Terlevich R., Davies R.L., Faber S.M., Burstein D., 1981, *MNRAS*, 196, 381
 Thomas D., Maraston C., Bender R., 2002, *Ap&SS*, 281, 371
 Thomas D., Maraston C., Bender R., 2003, *MNRAS*, 339, 897
 Thomas D., Maraston C., Bender R., de Oliveira C.M., 2005, *ApJ*, 621, 673

- Trager S.C., Worthey G., Faber S.M., Burstein D.,
González J.J., 1998, ApJS, 116, 1
- Trager S.C., Faber S.M., Worthey G., González J.J., 2000,
AJ, 119, 1645
- Tully R.B., Fisher J.R., 1977, A&A, 54, 661T
- Vazdekis A., Casuso E., Peletier R.F., Beckman J.E., 1996,
ApJS, 106, 307
- Vazdekis A., 1999, ApJ, 513, 224
- Vazdekis A., Kuntschner H., Davies R.L., Arimoto N.,
Nakamura O., Peletier R., 2001, ApJ, 551L, 127
- Worthey G., P.hD. Thesis, University of California, Santa
Cruz
- Worthey G., Faber S.M., Gonzalez J.J., 1992, ApJ, 398, 69
- Worthey G., Faber S.M., González J.J., Burstein D., 1994,
ApJS, 94, 687
- Worthey G., Ottaviani D.L., 1997, ApJS, 111, 377
- Worthey G., Collobert M., 2003, ApJ, 586, 17

APPENDIX A: TABLES

In this appendix we include tables with different parameters for each galaxy of our sample.

Table A1 includes central absorption line indices measured at 3 Å resolution for all our galaxies while Table A2 presents similar values measured at Lick resolution.

In Table A3, central luminosity-weighted ages and [Fe/H] are presented for our galaxies by using different [Fe/H] indicators, H β as the age indicator and Bruzual & Charlot (2003) models at Lick resolution.

Table A1. Central Line Indices measured at 3 Å resolution of S0 galaxies in Fornax.

Name	[MgFe]'	⟨Fe⟩	Hβ	Fe5015	Mg ₁	Mg ₂	Mgb	Fe5270	Fe5335	Fe5406	Fe5709	Fe5782
(1)	[Å] (2)	[Å] (3)	[Å] (4)	[Å] (5)	[mag] (6)	[mag] (7)	[Å] (8)	[Å] (9)	[Å] (10)	[Å] (11)	[Å] (12)	[Å] (13)
CENTRAL												
NGC 1380	4.14 (0.04)	3.53 (0.03)	1.48 (0.04)	6.10 (0.08)	0.149 (0.001)	0.305 (0.001)	4.92 (0.03)	3.43 (0.04)	3.64 (0.04)	2.29 (0.03)	1.11 (0.03)	1.02 (0.03)
NGC 1381	3.71 (0.04)	3.09 (0.03)	1.65 (0.04)	5.46 (0.08)	0.113 (0.001)	0.263 (0.001)	4.42 (0.03)	3.14 (0.04)	3.04 (0.04)	2.03 (0.03)	1.16 (0.03)	0.87 (0.03)
NGC 1380A	3.18 (0.09)	2.99 (0.06)	2.91 (0.08)	5.68 (0.16)	0.058 (0.001)	0.183 (0.002)	3.33 (0.08)	3.10 (0.08)	2.88 (0.10)	1.77 (0.07)	0.98 (0.07)	0.86 (0.07)
NGC 1375	2.71 (0.08)	3.06 (0.06)	3.89 (0.09)	6.76 (0.17)	0.053 (0.001)	0.161 (0.002)	2.43 (0.08)	2.98 (0.08)	3.15 (0.09)	1.78 (0.06)	1.10 (0.05)	0.76 (0.05)
IC 1963	3.54 (0.08)	3.31 (0.05)	2.45 (0.07)	6.40 (0.14)	0.072 (0.001)	0.212 (0.001)	3.76 (0.07)	3.38 (0.07)	3.24 (0.08)	1.97 (0.06)	1.16 (0.05)	0.79 (0.05)
ESO 358–G006	2.59 (0.16)	2.61 (0.11)	2.35 (0.15)	4.75 (0.29)	0.039 (0.003)	0.142 (0.003)	2.51 (0.14)	2.75 (0.15)	2.48 (0.17)	1.52 (0.13)	1.01 (0.11)	0.58 (0.12)
ESO 358–G059	2.82 (0.07)	2.56 (0.05)	2.25 (0.06)	4.71 (0.12)	0.048 (0.001)	0.155 (0.001)	3.03 (0.06)	2.70 (0.06)	2.42 (0.07)	1.69 (0.05)	0.94 (0.05)	0.46 (0.05)
NGC 1316	3.73 (0.08)	3.28 (0.05)	2.16 (0.07)	5.96 (0.14)	0.094 (0.014)	0.228 (0.001)	4.26 (0.07)	3.26 (0.07)	3.30 (0.08)	2.07 (0.06)	1.04 (0.05)	1.02 (0.05)
ESO 359–G002	1.95 (0.15)	1.92 (0.11)	3.54 (0.13)	3.99 (0.26)	0.025 (0.011)	0.107 (0.003)	2.01 (0.13)	1.87 (0.14)	1.97 (0.16)	1.12 (0.12)	0.57 (0.11)	0.63 (0.11)

Notes: From (2) to (13), 1 σ rms errors between " () "; Col (1), name; Col (2), [MgFe]' combined index (González 1993; Thomas, Maraston & Bender 2003); Col (3), ⟨Fe⟩ combined index (Gorgas, Efstathiou & Aragón-Salamanca 1990); Col (4), Hβ index; Col (5), Fe5015 index; Col (6), Mg₁ index in magnitudes; Col (7), Mg₂ index in magnitudes; Col (8), Mgb index; Col (9), Fe5270 index; Col (10), Fe5335 index; Col (11), Fe5406 index; Col (12), Fe5709 index; Col (13), Fe5782 index.

Table A2. Central Line Indices measured at Lick resolution of S0 galaxies in Fornax.

Name	[MgFe]'	⟨Fe⟩	H β	Fe5015	Mg ₁	Mg ₂	Mgb	Fe5270	Fe5335	Fe5406	Fe5709	Fe5782
(1)	[Å]	[Å]	[Å]	[Å]	[mag]	[mag]	[Å]	[Å]	[Å]	[Å]	[Å]	[Å]
(1)	(2)	(3)	(4)	(5)	(6)	(7)	(8)	(9)	(10)	(11)	(12)	(13)
CENTRAL												
NGC 1380	3.82 (0.04)	3.01 (0.03)	1.47 (0.04)	5.13 (0.08)	0.162 ^a (0.007)	0.322 ^a (0.007)	4.86 (0.04)	3.02 (0.04)	3.00 (0.04)	1.97 (0.03)	1.00 (0.03)	0.83 (0.03)
NGC 1381	3.40 (0.04)	2.70 (0.03)	1.65 (0.04)	4.83 (0.08)	0.128 ^a (0.007)	0.283 ^a (0.007)	4.20 (0.04)	2.81 (0.04)	2.60 (0.05)	1.75 (0.03)	1.05 (0.03)	0.75 (0.03)
NGC 1380A	2.88 (0.09)	2.65 (0.06)	2.78 (0.08)	4.69 (0.16)	0.075 ^a (0.011)	0.204 ^a (0.007)	3.07 (0.08)	2.79 (0.09)	2.51 (0.10)	1.53 (0.07)	0.90 (0.07)	0.66 (0.07)
NGC 1375	2.52 (0.07)	2.63 (0.05)	3.47 (0.07)	5.24 (0.14)	0.057 ^a (0.011)	0.169 ^a (0.007)	2.39 (0.07)	2.69 (0.07)	2.57 (0.08)	1.55 (0.00.1626)	1.00 (0.05)	0.68 (0.05)
IC 1963	3.22 (0.08)	2.87 (0.05)	2.26 (0.07)	5.27 (0.14)	0.089 ^a (0.015)	0.233 ^a (0.007)	3.56 (0.07)	3.00 (0.07)	2.75 (0.08)	1.71 (0.06)	1.02 (0.05)	0.64 (0.05)
ESO 358–G006	2.41 (0.16)	2.23 (0.12)	2.11 (0.15)	3.97 (0.29)	0.054 ^a (0.028)	0.161 ^a (0.008)	2.51 (0.14)	2.44 (0.15)	2.03 (0.18)	1.35 (0.13)	0.89 (0.12)	0.50 (0.12)
ESO 358–G059	2.53 (0.07)	2.25 (0.05)	2.16 (0.06)	3.92 (0.13)	0.065 ^a (0.008)	0.178 ^a (0.007)	2.76 (0.06)	2.40 (0.06)	2.10 (0.07)	1.47 (0.05)	0.87 (0.05)	0.34 (0.05)
NGC 1316	3.22 (0.08)	2.76 (0.05)	2.11 (0.07)	5.15 (0.14)	0.111 ^a (0.015)	0.250 ^a (0.007)	3.74 (0.07)	2.77 (0.07)	2.75 (0.08)	1.66 (0.06)	0.93 (0.05)	0.77 (0.05)
ESO 359–G002	1.70 (0.14)	1.54 (0.10)	3.32 (0.13)	3.15 (0.25)	0.039 ^a (0.012)	0.123 ^a (0.008)	1.86 (0.13)	1.58 (0.14)	1.51 (0.16)	1.00 (0.12)	0.52 (0.11)	0.51 (0.11)

Notes: From (2) to (13), 1σ rms errors between $''()$; Col (1), name; Col (2), [MgFe]' combined index (González 1993; Thomas, Maraston & Bender 2003); Col (3), ⟨Fe⟩ combined index (Gorgas, Efstathiou & Aragón-Salamanca 1990); Col (4), H β index; Col (5), Fe5015 index; Col (6), Mg₁ index in magnitudes; Col (7), Mg₂ index in magnitudes; Col (8), Mgb index; Col (9), Fe5270 index; Col (10), Fe5335 index; Col (11), Fe5406 index; Col (12), Fe5709 index; Col (13), Fe5782 index.

(^a) An additive spectrophotometric correction to the Lick system was applied to the indices Mg₁ and Mg₂.

Table A3. Central Ages and Metallicities using line indices at Lick resolution for S0 galaxies in Fornax.

Name	$\log(\text{Age})_{[\text{MgFe}]'}$ [yr]	$[\text{Fe}/\text{H}]_{[\text{MgFe}]'}$ [dex]	$\log(\text{Age})_{\langle\text{Fe}\rangle}$ [yr]	$[\text{Fe}/\text{H}]_{\langle\text{Fe}\rangle}$ [dex]	$\log(\text{Age})_{\text{Mgb}}$ [yr]	$[\text{Fe}/\text{H}]_{\text{Mgb}}$ [dex]	$\log(\text{Age})_{\text{Fe5709}}$ [yr]	$[\text{Fe}/\text{H}]_{\text{Fe5709}}$ [dex]
(1)	(2)	(3)	(4)	(5)	(6)	(7)	(8)	(9)
NGC 1380	10.09 $^{+0.06}_{-0.05}$	0.23 $^{+0.05}_{-0.05}$	10.21 $^{+0.06}_{-0.06}$	-0.02 $^{+0.03}_{-0.03}$	9.95 $^{+0.05}_{-0.05}$	0.63 $^{+0.06}_{-0.06}$	10.23 $^{+0.06}_{-0.05}$	-0.05 $^{+0.05}_{-0.05}$
NGC 1381	9.99 $^{+0.05}_{-0.05}$	0.06 $^{+0.05}_{-0.05}$	10.10 $^{+0.06}_{-0.05}$	-0.17 $^{+0.03}_{-0.04}$	9.89 $^{+0.06}_{-0.06}$	0.34 $^{+0.07}_{-0.06}$	9.99 $^{+0.04}_{-0.04}$	0.06 $^{+0.06}_{-0.06}$
NGC 1380A	9.16 $^{+0.06}_{-0.06}$	0.53 $^{+0.12}_{-0.11}$	9.23 $^{+0.04}_{-0.04}$	0.33 $^{+0.06}_{-0.06}$	9.08 $^{+0.08}_{-0.08}$	0.77 $^{+0.16}_{-0.15}$	9.30 $^{+0.04}_{-0.04}$	0.07 $^{+0.15}_{-0.17}$
NGC 1375	8.87 $^{+0.05}_{-0.05}$	0.67 $^{+0.10}_{-0.10}$	8.91 $^{+0.04}_{-0.04}$	0.56 $^{+0.04}_{-0.04}$	8.84 $^{+0.06}_{-0.07}$	0.78 $^{+0.14}_{-0.13}$	8.97 $^{+0.04}_{-0.05}$	0.36 $^{+0.08}_{-0.09}$
IC 1963	9.41 $^{+0.05}_{-0.06}$	0.42 $^{+0.10}_{-0.10}$	9.43 $^{+0.06}_{-0.05}$	0.27 $^{+0.05}_{-0.05}$	9.36 $^{+0.07}_{-0.07}$	0.59 $^{+0.14}_{-0.13}$	9.47 $^{+0.07}_{-0.06}$	0.14 $^{+0.11}_{-0.11}$
ESO 358-G006	9.81 $^{+0.14}_{-0.13}$	-0.37 $^{+0.16}_{-0.15}$	9.79 $^{+0.13}_{-0.12}$	-0.30 $^{+0.12}_{-0.12}$	9.83 $^{+0.14}_{-0.13}$	-0.43 $^{+0.14}_{-0.13}$	9.72 $^{+0.15}_{-0.14}$	-0.10 $^{+0.25}_{-0.30}$
ESO 358-G059	9.74 $^{+0.06}_{-0.07}$	-0.25 $^{+0.07}_{-0.07}$	9.75 $^{+0.06}_{-0.06}$	-0.26 $^{+0.05}_{-0.05}$	9.74 $^{+0.07}_{-0.08}$	-0.23 $^{+0.07}_{-0.06}$	9.70 $^{+0.06}_{-0.06}$	-0.13 $^{+0.11}_{-0.12}$
NGC 1316	9.54 $^{+0.09}_{-0.10}$	0.28 $^{+0.09}_{-0.09}$	9.61 $^{+0.07}_{-0.08}$	0.12 $^{+0.05}_{-0.05}$	9.41 $^{+0.09}_{-0.07}$	0.57 $^{+0.13}_{-0.13}$	9.69 $^{+0.08}_{-0.08}$	-0.04 $^{+0.11}_{-0.12}$
ESO 359-G002	9.19 $^{+0.05}_{-0.05}$	-0.27 $^{+0.16}_{-0.15}$	9.23 $^{+0.05}_{-0.05}$	-0.45 $^{+0.10}_{-0.10}$	9.13 $^{+0.06}_{-0.07}$	-0.01 $^{+0.17}_{-0.15}$	9.37 $^{+0.17}_{-0.13}$	-0.89 $^{+0.37}_{-0.42}$

Notes: From (2) to (9), 99% confidence intervals are presented. Col (1), name; Col (2) (3), age and metallicity, estimated using Bruzual & Charlot (2003) simple stellar population models at Lick resolution and $[\text{MgFe}]'$ as metallicity indicator; Col (4) (5), age and metallicity, estimated using $\langle\text{Fe}\rangle$ as metallicity indicator; Col (6) (7), age and metallicity, estimated using Mgb as metallicity indicator; Col (8) (9), age and metallicity, estimated using Fe5709 as metallicity indicator.

This paper has been typeset from a \TeX / \LaTeX file prepared
by the author.